Synergistic impact of simultaneously assimilating radar- and radiometer-based soil moisture retrievals on the performance of numerical weather prediction systems

Yonghwan Kwon[a*], Sanghee Jun[a], Hyunglok Kim[b], Kyung-Hee Seol[a], In-Hyuk Kwon[a], Eunkyu Kim[a], Sujeong Cho[a]

[a]Korea Institute of Atmospheric Prediction System, Seoul 07071, South Korea

[b]Department of Environment and Energy Engineering, Gwangju Institute of Science and Technology (GIST), Gwangju 61005, South Korea

[*]To whom correspondence may be addressed (yhkwon@kiaps.org).

Revised manuscript submitted to ***Hydrology and Earth System Sciences***

Abstract

The combined use of independent soil moisture data from radar and radiometer measurements in data assimilation (DA) systems is expected to yield synergistic performance gains due to their complementary strengths. This study evaluates the impact of simultaneously assimilating soil moisture retrievals from ASCAT (Advanced SCATterometer) and SMAP (Soil Moisture Active Passive) into the Korean Integrated Model (KIM) using a weakly coupled DA framework based on the National Aeronautics and Space Administration's Land Information System (LIS). The Noah land surface model (LSM) within LIS, which is the same as that used in KIM, is used to simulate land surface states and assimilate soil moisture retrievals. The impact of soil moisture DA is evaluated using independent reference datasets, assessing its influence on soil moisture analysis and numerical weather prediction performance. Overall, assimilating ASCAT or SMAP soil moisture data into the LSM improves global soil moisture analysis accuracy by 4.0% and 10.5%, respectively, compared to the control case without soil moisture DA, achieving the most significant enhancements in croplands. Relative to single-sensor soil moisture DA, multi-sensor soil moisture DA yields more balanced skill enhancements for both specific humidity and air temperature analyses and forecasts. The most pronounced synergistic improvements by simultaneously assimilating both soil moisture products are observed in the 2-m air temperature analysis and forecast, especially when both soil moisture products have a positive impact. The results also demonstrate that precipitation forecast skill, particularly in predicting precipitation events, can be enhanced by constraining the modeled soil moisture with multiple soil moisture retrievals from different sources. This paper discusses remaining

issues for future studies to further improve the weather prediction performance of the KIM-LIS multi-sensor soil moisture DA system.

Key words: soil moisture data assimilation, multi-sensor, Korean Integrated Model, Land Information System, numerical weather prediction, land-atmosphere coupled system

1. Introduction

Soil moisture is one of the decisive land surface state variables that control land-atmosphere interactions associated with water and energy cycles (Gentine et al., 2011; Koster et al., 2004; Tuttle and Salvucci, 2016) and that determine surface water infiltration, percolation, and runoff (Assouline, 2013; Orth and Seneviratne, 2013). Many studies underline the importance of accurate knowledge of the spatial and temporal soil moisture variability for various hydrometeorological applications (e.g., Jalilvand et al., 2019; Shin and Jung, 2014; Wanders et al., 2014; Yuan et al., 2011). Because of the long-memory effect of soil moisture, proper soil moisture initialization is a prominent part of numerical weather prediction (NWP), particularly in the lower atmosphere (Dirmeyer and Halder, 2016; Drusch and Viterbo, 2007; Jun et al., 2021; Koster et al., 2010; Kwon et al., 2024; van den Hurk et al., 2012).

As a viable method to produce spatially and temporally complete, observation-constrained estimates of soil moisture profiles (Bolten et al., 2010; Reichle et al., 2002a), assimilating satellite-based soil moisture data into land surface models (LSMs) has been widely explored. Soil moisture data assimilation (DA) optimally merges remotely-sensed near-surface soil

45 moisture observations with modeled soil moisture estimates based on their respective
46 uncertainties (Kumar et al., 2008a; Reichle et al., 2008), and it can generate soil moisture
47 estimates superior to either observations or models alone when the relative size of the
48 uncertainties is properly characterized (Liu et al., 2011; Blyverket et al., 2019). A number of
49 studies have applied soil moisture DA to improve flood and drought forecasts (e.g., Azimi et
50 al., 2020; Gavahi et al., 2022; Laiolo et al., 2016), streamflow and runoff predictions (e.g.,
51 Baugh et al., 2020; Brocca et al., 2010; Lievens et al., 2016), irrigation characterization (e.g.,
52 Kwon et al., 2022; Nair and Indu, 2019), and evaporative flux estimates (e.g., Li et al., 2020;
53 Pipunic et al., 2013). In particular, it has been demonstrated that the assimilation of satellite-
54 based soil moisture retrievals into LSMs that are coupled to atmospheric models has a
55 positive impact on weather forecast skill (e.g., Draper and Reichle, 2019; Jun et al., 2021;
56 Kwon et al., 2024; Lin and Pu, 2020; Lodh et al., 2022; Yin et al., 2019).
57 In addition to DA methods, a variety of alternative data fusion techniques have been
58 widely explored to integrate soil moisture information from different sources, including
59 remote sensing products, in-situ measurements, model simulations, and reanalysis datasets.
60 One group of approaches relies on statistical methods (e.g., Min et al., 2022; Wang et al.,
61 2021; Xie et al., 2022), such as unweighted averaging, linear weight fusion, and emergent
62 constraint. Another group leverages machine learning (e.g., Huang et al., 2023; Lamichhane
63 et al., 2025; Long et al., 2019; Zhang et al., 2022, Zeng et al., 2024) and deep learning
64 techniques (e.g., Fuentes et al., 2022; Huang et al., 2022; Jiang et al., 2025; Singh and Gaurav,
65 2023; van der Schalie et al., 2018). These machine learning and deep learning approaches are
66 rapidly gaining prominence because of their ability to incorporate diverse data sources and to

capture complex, nonlinear relationships between datasets (Huang et al, 2022; Zeng et al., 2024). While different fusion approaches have distinct strengths and limitations, this study is devoted to DA methods, with the goal of improving model-based soil moisture estimates that interact with atmospheric processes in operational land-atmosphere coupled systems, thereby enhancing weather forecasts.

Microwave satellite systems provide useful information to retrieve surface soil moisture data at the global scale owing to their sensitivity to soil dielectric properties that mainly depend on soil water content and surface roughness (Schmugge et al., 1986). Many satellite soil moisture products have been generated from microwave observations at different frequencies (i.e., X, C and L-band) using various retrieval algorithms in different systems during the past several decades (Kumar et al., 2019; Nair and Indu, 2018). Among them, the Advanced SCATterometer (ASCAT) (e.g., Bartalis et al., 2007; Wagner et al., 2013), Soil Moisture Active Passive (SMAP) (e.g., Chan et al., 2018; O'Neill et al., 2021), and Soil Moisture and Ocean Salinity (SMOS) (e.g., Kerr et al., 2012) are relatively modern sensors that have been widely used in soil moisture DA studies (e.g., Blyverket et al., 2019; Jun et al., 2021; Khaki and Awange, 2019; Kolassa et al., 2017; Kumar et al., 2019; Kwon et al., 2022, 2024; Nair and Indu, 2019; Renzullo et al., 2014; Seo et al., 2021; Tangdamrongsub et al., 2020). In addition, most recently, Nguyen et al. (2025) have demonstrated the usefulness of soil moisture retrievals based on signals from the Global Navigation Satellite Systems. Kumar et al. (2019) report that soil moisture retrievals from these modern sensors exhibit better performance in DA systems than those from older sensors.

88 The present study focuses on the use of the ASCAT and SMAP soil moisture products to
89 improve modeled soil moisture estimates via assimilation. The ASCAT soil moisture product
90 is generated from active microwave backscatter measurements at C-band (5.3 GHz) while the
91 SMAP soil moisture data is based on passive microwave satellite systems, which utilize
92 naturally emitted brightness temperature from the Earth's surface at an L-band (1.4 GHz)
93 frequency. The C-band (i.e., ASCAT) and L-band (i.e., SMAP) sensors typically provide soil
94 moisture information for soil depth of 0–2 cm and 0–5 cm, respectively (Kim et al., 2018).
95 Compared to passive radiometers, radar observations (i.e., ASCAT) have smaller footprint
96 sizes (i.e., finer spatial resolutions) and thus provide better spatial details of soil moisture
97 (Nair and Indu, 2019). However, ASCAT has large uncertainties over regions of complex
98 topography due to multiple scattering effects (Dobson and Ulaby, 1986). In contrast,
99 radiometer (SMAP) observations are more sensitive to the presence of soil moisture than
100 active radars (Kolassa et al., 2017), but the accuracy of their soil moisture products is
101 strongly influenced by vegetation water content and surface temperature (Paloscia and
102 Pampaloni, 1988).
103 Because of their complementary advantages, better soil moisture estimates can be obtained
104 by assimilating the soil moisture data from multiple sources into the model-simulated soil
105 moisture within a DA system. There have been some efforts to synergistically combine
106 multiple active and passive observations for spatially and temporally improved soil moisture
107 retrievals such as the European Space Agency Climate Change Initiative (ESA CCI; Dorigo
108 et al., 2017). In addition, one of the key goals of the SMAP mission was to utilize both active
109 and passive sensors on the same satellite platform to retrieve high spatial resolution global

near-surface soil moisture data with great accuracy (Entekhabi et al., 2010). However, due to mechanical malfunction of the SMAP radar, alternative radar observations from other satellites (e.g., Sentinel-1) have been combined with the SMAP radiometer data to maintain data continuity (Das et al., 2019). Meanwhile, Kolassa et al. (2017) and Nair and Indu (2019) demonstrate that simultaneously assimilating individual radar- and radiometer-based soil moisture retrievals achieves comparable overall performance to the assimilation of the blended (i.e., radar + radiometer) soil moisture products. In this study, we do not aim to retrieve or assimilate blended soil moisture products from multiple satellite measurements. Instead, we independently utilize soil moisture data from each sensor (i.e., ASCAT and SMAP) within a land-atmosphere coupled DA system, while also incorporating both observations separately rather than combining them spatially. This approach may provide a more effective way to account for the relative reliability of each sensor in soil moisture assimilation (Kolassa et al., 2017), and offers greater flexibility for assimilating various soil moisture products simultaneously in different combinations.

This study is built on a land-atmosphere coupled DA system, which consists of the Korean Integrated Model (KIM; Hong et al., 2018) and the National Aeronautics and Space Administration (NASA) Land Information System (LIS; Kumar et al., 2006, 2008b; Peters-Lidard et al., 2007). Hereafter, this system is referred to as the KIM-LIS coupled system. As an operational global NWP model at the Korea Meteorological Administration, KIM has been developed by the Korea Institute of Atmospheric Prediction Systems (KIAPS). KIM has capabilities of conducting short-to-medium-range and extended-range weather forecasts, and of implementing atmospheric DA to generate improved atmospheric initial conditions for the

forecasts (Kwon et al., 2018). Land DA in the current Korea Meteorological Administration's operational NWP system is based on the KIM-LIS coupled system and ingests the ASCAT soil moisture retrievals to constrain the modeled soil moisture (Jun et al., 2021). Recently Kwon et al. (2024) have demonstrated the feasibility of assimilating the SMAP soil moisture retrievals into the Noah LSM (Ek et al., 2003) within the KIM-LIS system to enhance the global soil moisture estimates and weather forecast performance of KIM.

While several studies have explored the simultaneous use of radar and radiometer-based soil moisture data in offline land DA systems, mainly to improve soil moisture estimates and associated hydrological processes (e.g., Draper et al., 2012; Khaki and Awange, 2019; Khaki et al., 2019, 2020; Kolassa et al., 2017; Kumar et al., 2019; Nair and Indu, 2019; Renzullo et al., 2014; Seo et al., 2021; Tangdamrongsub et al., 2020), only a few have investigated their impacts on atmospheric forecasts in land-atmosphere coupled NWP systems (e.g., de Rosnay et al., 2022; Draper and Reichle, 2019; Fairbairn et al., 2024). Even among studies using coupled forecast systems, most assimilate only ASCAT and SMOS together, despite evidence that SMAP provides high-quality soil moisture data (e.g., Bhuiyan et al., 2018; Chan et al., 2018; Colliander et al., 2017) and often outperforms other sensors (Kumar et al., 2018). In this regard, the novelty of this study is the combined use of ASCAT and SMAP soil moisture products in the KIM-LIS-based land-atmosphere coupled DA system, demonstrating their feasibility.

The present study aims to evaluate the relative (individual) and combined performance of C-band radar-based (i.e., ASCAT) and L-band radiometer-based (i.e., SMAP) surface soil moisture products in improving the global soil moisture analysis and atmospheric

analysis/forecast via assimilation within the KIM-LIS coupled system. We first assimilate each soil moisture product individually into the Noah LSM in the KIM-LIS system over the global domain, and compare their respective performance gains. The synergistic impacts of simultaneously assimilating the ASCAT and SMAP soil moisture retrievals on the global estimates of lower atmospheric variables are then investigated.

2. KIM-LIS-based weakly coupled DA system

The KIM-LIS system (Jun et al., 2021; Kwon et al., 2024) is a weakly coupled DA system, in which the land analysis and atmospheric analysis are implemented independently (Figure 1). The present study uses the KIM version 3.9 and LIS version 7.4, the same versions as those used in Kwon et al. (2024). KIM (Hong et al., 2018) is composed of a global non-hydrostatic dynamical core using a cubed-sphere grid system with up to 91 vertical levels on a hybrid-sigma coordinate system (Song et al., 2017; Kwon et al., 2018). LIS (Kumar et al., 2006, 2008b; Peters-Lidard et al., 2007) is a land surface hydrological modeling and DA system where various LSMs, DA schemes, and surface coordinate systems are available for different applications. In this study, the latitude-longitude grid system is used for LIS.

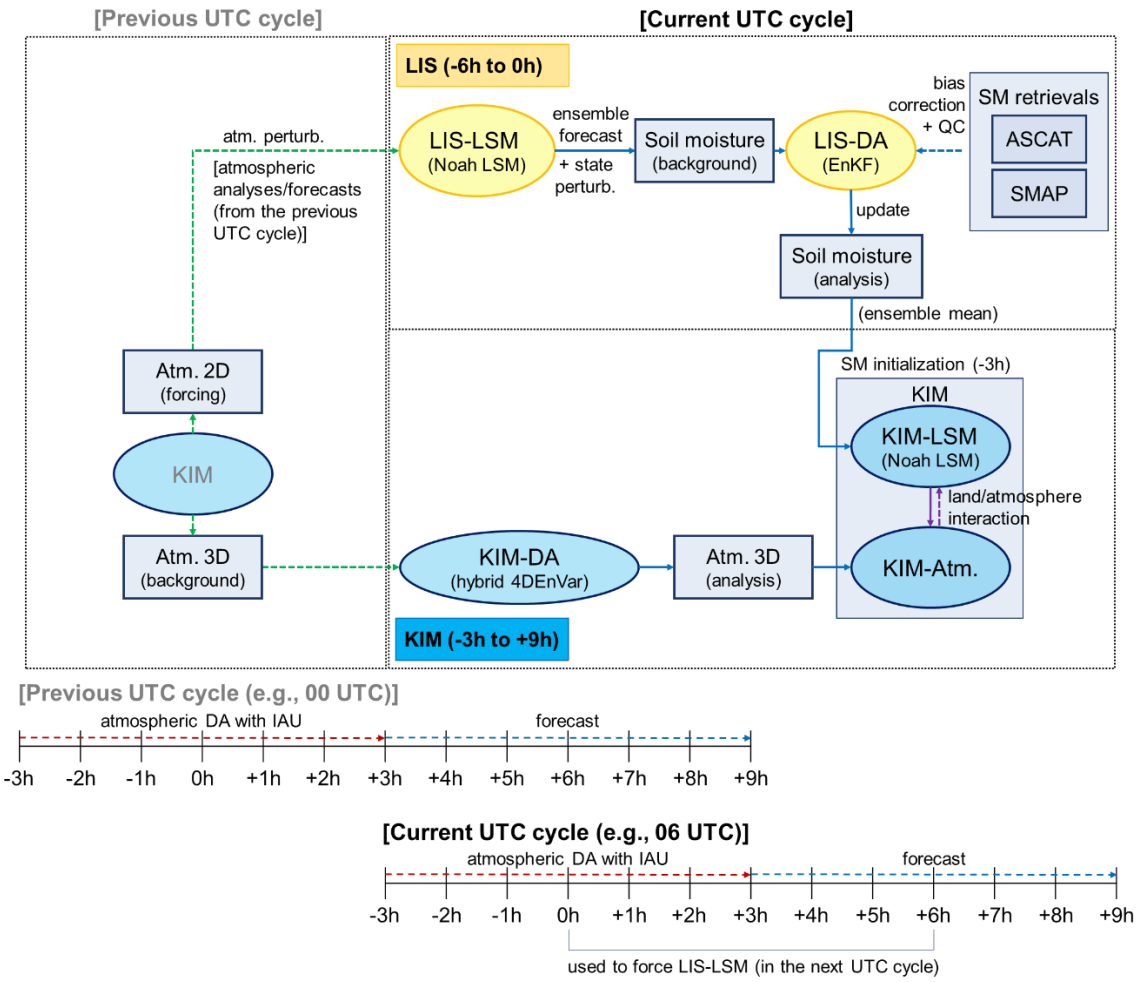

Figure 1. Schematic diagram of the KIM-LIS-based land-atmosphere weakly coupled data assimilation (DA) system. The figure outlines the process flow between KIM and LIS in one UTC cycle that is performed four times (i.e., 00, 06, 12, and 18 UTC cycles) a day. (IAU: incremental analysis update, QC: quality control)

KIM and LIS employ separate versions of the Noah LSM, referred to as KIM-LSM and LIS-LSM, respectively, in Figure 1 to simulate land-surface hydrological processes. In the Noah LSM (Ek et al., 2003), a soil column (2-m total depth) is discretized into four layers with the standard thickness of 0.1 m, 0.3 m, 0.6 m, and 1.0 m from surface to bottom for estimation of soil moisture and soil temperature. The Noah LSM estimates soil moisture and

soil temperature based on the diffusivity form of the Richards equation and one-dimensional thermal diffusion equation, respectively. Surface water infiltration is estimated following Schaake et al. (1996) by considering the frozen soil effects. Simulations of latent heat flux and evapotranspiration rely on the formulation of the Penman equation. The original Noah version of KIM-LIS is 2.7.1, but it has undergone many updates based on later versions of the Noah LSM with additional modifications to physical parameterizations and land surface inputs to achieve optimal performance of KIM (Koo et al., 2017). As in Jun et al. (2021) and Kwon et al. (2024), the Noah LSM version 3.3 implemented within LIS is used for LIS-LSM by applying the same modifications to ensure consistency between KIM-LSM and LIS-LSM.

The KIM-LIS coupled system conducts a forecast/analysis cycle every 6 hours [i.e., 00, 06, 12, and 18 Coordinated Universal Time (UTC) cycles] where KIM and LIS run for time windows of 12 hours (i.e., −3 h to +9 h) and 6 hours (i.e., −6 h to 0 h), respectively, as outlined in Figure 1. LIS-LSM (i.e., Noah LSM) creates an ensemble of background (prior) soil moisture estimates forced by atmospheric fields from the previous UTC cycle (0 h to +6 h) KIM analysis/forecast, which are remapped from the cubed-sphere grid to the latitude-longitude grid and perturbed by adding Gaussian random perturbations. Additional random perturbations are imposed on the prior soil moisture estimates, which are then merged with remotely-sensed soil moisture retrievals using the ensemble Kalman filter (EnKF) method (Evensen, 1994; Reichle et al., 2002b) to generate the soil moisture analysis. This sequential EnKF procedure (i.e., soil moisture forecast and analysis) is performed from −6 h to 0 h in the current UTC cycle. LIS writes land outputs every 3 hours (i.e., at −3 h and 0 h) and generates a restart file at 0 h. The restart file contains the complete set of model state

variables at that time, enabling LIS-LSM to be consistently re-initialized in the subsequent UTC cycle. The soil moisture analysis from LIS at −3 h is remapped from the latitude-longitude grid to the cubed-sphere grid, and is used to initialize the soil moisture conditions of KIM-LSM that provides land boundary conditions for the KIM forecast and analysis from −3 h to +9 h in the current UTC cycle. The atmospheric analysis is performed based on the hybrid four-dimensional ensemble variational (hybrid 4DEnVar) DA method (Song et al., 2017; Kwon et al., 2018). To minimize the initialization shock resulting from the atmospheric DA, the four-dimensional incremental analysis update (4DIAU; Lorenc et al.,2015) is employed within an atmospheric assimilation window (i.e., −3 h to + 3h). KIM is further run without DA until +9 h, and the KIM analysis/forecasts from 0 h to +6 h in the current UTC cycle are then used for the next UTC cycle LIS implementation.

Although the remapping procedures required to share information between KIM and LIS may introduce some error, Jun et al. (2021) and Kwon et al. (2024) have demonstrated that soil moisture DA based on the KIM-LIS system provides beneficial impacts on improving the weather forecast performance of KIM. In addition, the KIM-LIS coupled system, which employs the LIS-based land DA, has several advantages: (1) it can readily leverage the existing land DA functions of LIS, and (2) it allows straightforward implementation of new land DA developments due to LIS's extensible framework.

3. Satellite-based soil moisture retrievals

We assimilate the satellite-based near-surface soil moisture retrievals from ASCAT and SMAP individually and together into the Noah LSM to constrain the modeled soil moisture estimates. A brief explanation of the soil moisture products is given below.

3.1. Active soil moisture product: ASCAT

ASCAT is a real aperture radar onboard the Meteorological Operational (MetOp) satellites (i.e., MetOp-A, MetOp-B, and MetOp-C), and measures radar backscatter at C-band (5.3 GHz) VV (vertical transmit vertical receive) polarization (Wagner et al., 2013). The MetOp satellites follow a near-polar sun-synchronous orbit, and their equator crossing times are 9:30 am/pm local solar time (LST) for the descending and ascending overpasses, respectively, with a revisit frequency of 1–3 days. Although ASCAT was originally designed to monitor wind direction and speed over the ocean, it has also been effectively utilized to retrieve soil moisture over land due to its multiple-viewing capabilities and its sensitivity to soil moisture variability (Wagner et al., 2013). The ASCAT soil moisture is retrieved based on the Vienna University of Technology (TU Wien) change detection algorithm (Wagner et al., 1999, 2010), and provides an estimate of the degree of water saturation (ranging between 0 and 100%) of the top 0–2 cm soil layer.

We use the MetOp-B/C ASCAT near-real time soil moisture product at 12.5 km swath grid. The soil moisture product used in this study was obtained directly from the European Organisation for the Exploitation of Meteorological Satellites (EUMETSAT) for use in the Korea Meteorological Administration's operational weather prediction system while the same

product can be downloaded from the EUMETSAT Earth Observation Portal (https://eoportal.eumetsat.int).

3.2. Passive soil moisture product: SMAP

Unlike ASCAT, the SMAP mission is specifically designed for global soil moisture monitoring based on L-band (1.4 GHz) passive microwave radiometer measurements (Entekhabi et al., 2010). The SMAP satellite is in sun-synchronous orbits at approximately 685 km altitudes with a local equator-crossing time of 6 am (descending) and 6 pm (ascending) and a revisit cycle of 2–3 days. It provides volumetric soil moisture (in m^3 m^{-3}) for a soil depth of 0–5 cm from the surface.

The present study uses the SMAP Level 2 (L2) Radiometer Half-Orbit 36 km Equal Area Scalable Earth (EASE)–Grid soil moisture data (SPL2SMP version 9, O'Neill et al., 2021), which is obtained from the National Snow and Ice Data Center (NSIDC, https://n5eil01u.ecs.nsidc.org/SMAP/SPL2SMP.009/). The SMAP soil moisture retrievals based on the Dual Channel Algorithm (DCA, Chaubell et al., 2020) are assimilated. DCA uses both horizontally and vertically polarized brightness temperature measurements and is the current baseline retrieval algorithm of the SMAP soil moisture product (Chan and Dunbar, 2021).

3.3. Bias correction of the soil moisture data

Typical DA algorithms are designed to correct random errors under the assumption of unbiased state estimates between models and observations (Dee and da Silva, 1998).

271 However, there are generally large systematic discrepancies between modeled and satellite-
272 retrieved soil moisture because of their different representations of soil moisture associated
273 with the geophysical definition and horizontal/vertical scales (Koster et al., 2009; Kumar et
274 al., 2019). Therefore, soil moisture DA systems essentially employ appropriate bias
275 correction strategies to remove these systematic biases prior to assimilation, and thus to
276 comply with the DA assumption of unbiased models and observations (Kolassa et al., 2017;
277 Reichle and Koster, 2004). In this study, bias correction is implemented differently for the
278 ASCAT and SMAP soil moisture products. That is, we apply cumulative distribution function
279 (CDF) matching (Reichle and Koster 2004) and anomaly correction methods (Kwon et al.,
280 2022) to assimilate the ASCAT and SMAP soil moisture retrievals, respectively, into the
281 Noah LSM within the KIM-LIS coupled system. The use of the anomaly correction method
282 for SMAP follows our previous investigations (Kwon et al., 2022, 2024) aiming to minimize
283 the loss of useful information from the original data through bias correction. In contrast,
284 traditional CDF matching is applied to ASCAT, since the anomaly correction method is not
285 applicable due to difference in soil moisture data type between ASCAT (soil wetness index)
286 and the model (volumetric soil moisture in $m^3\ m^{-3}$). Further details are provided in the
287 following two paragraphs.

288 The CDF matching is a commonly used bias correction method in soil moisture DA.
289 Through the CDF matching, in this study, the ASCAT soil wetness index data are
290 transformed to volumetric soil moisture ($m^3\ m^{-3}$) by correcting all the statistical moments of
291 the original ASCAT data to those of the Noah-simulated soil moisture. Existing soil moisture
292 DA studies use two different CDF matching approaches. One uses a lumped CDF computed

using all seasons data (i.e., pixel-wise single CDF for each data type) (e.g., Draper et al., 2011, 2012; Kumar et al., 2009, 2014; Reichle et al., 2007) while the other uses monthly-stratified CDFs (i.e., pixel-wise 12 CDFs for each data type) (e.g., Jun et al., 2021; Kumar et al., 2015; Kwon et al., 2022, 2024; Santanello Jr et al., 2016). Kumar et al. (2015) and Santanello Jr et al., (2016) suggest using the monthly CDF rather than the lumped CDF to mitigate spurious statistical artifacts in the bias-corrected soil moisture by the CDF matching. Kwon et al. (2024) show that abnormal fluctuations are witnessed in the lumped CDF-based rescaled soil moisture, particularly in dry periods, and Kwon et al. (2022) demonstrate that soil moisture DA employing the monthly CDF achieves better soil moisture analysis than that applying the lumped CDF matching. Based on these previous findings, we implement the monthly CDF matching for the ASCAT soil moisture DA.

The anomaly correction method, proposed by Kwon et al. (2022), is a simpler alternative to traditional bias correction approaches. It aims to reduce the reliance of DA systems on rescaling methods like the CDF matching, which is known to cause significant information loss in the original soil moisture data, especially when human-induced processes (e.g., irrigation activities), poorly represented in models, are the dominant source of systematic discrepancies between observations and models (Kumar et al., 2015; Nearing et al., 2018). Instead of rescaling the SMAP soil moisture retrievals, the anomaly correction approach obtains the soil moisture temporal variability (i.e., anomaly) information by subtracting the long-term soil moisture mean from the original SMAP data. The extracted SMAP soil moisture anomaly is added to the long-term mean of the modeled soil moisture, which is then assimilated into the LSM. The anomaly correction assumes that the systematic bias between

observations and models is dominated by the climatological mean difference and higher moment (e.g., standard deviation) differences are negligible. Kwon et al. (2022) and Kwon et al. (2024) demonstrate that the SMAP soil moisture data and Noah-simulated soil moisture satisfy this underlying assumption over the continental United States and global domain, respectively. In particular, Kwon et al. (2024) show that the anomaly correction-based SMAP soil moisture DA is effective in improving the global soil moisture estimates and weather forecast skill of the KIM-LIS coupled system that employs the Noah LSM.

3.4. Quality control of the soil moisture data

The ASCAT and SMAP soil moisture retrievals undergo quality control before DA by removing inaccurate or uncertain soil moisture observations based on strategies employed in previous soil moisture DA studies (e.g., Blyverket et al., 2019; Draper et al., 2012; Ferguson et al., 2020; Jun et al., 2021; Kolassa et al., 2017; Kumar et al., 2014, 2019; Kwon et al., 2022, 2024; Nair and Indu, 2019). Firstly, before bias correction, the soil moisture data are discarded when the data quality flags provided with each soil moisture product indicate that the data accuracy is impacted by open water bodies, dense vegetation, urban areas, precipitation, snow cover, frozen ground, complex topography, or anthropogenic Radio Frequency Interference (RFI). Especially, the ASCAT soil moisture retrievals are assimilated only when the Estimated Soil Moisture Error (ESME) is less than 16%, and the topographic complexity and wetland fraction are below 20% and 15%, respectively, as applied in Jun et al. (2021). These uncertainty thresholds are slightly higher than those used in Draper et al. (2012)

and Kolassa et al. (2017) for the purpose of utilizing more data in a near-real time operational DA system.

Secondly, the model-based quality control is additionally applied to both ASCAT and SMAP after bias correction. Specifically, assimilation of ASCAT and SMAP soil moisture into the Noah LSM is not performed in the case that (1) model background estimates indicate active precipitation events or frozen/snow-covered soil conditions, that (2) the model land cover type and green vegetation fraction inputs from the Moderate resolution imaging spectroradiometer (MODIS) International Geosphere-Biosphere Programme (IGBP) data (Friedl et al., 2002) and the National Centers for Environmental Prediction (NCEP), respectively, indicate that a grid cell is classified as forests or has green vegetation fraction greater than 0.7, or that (3) bias-corrected soil moisture retrievals are close to wilting point or saturation.

4. DA methods

4.1. Atmospheric DA

Atmospheric DA in KIM is based on a hybrid four-dimensional ensemble variational (hybrid 4DEnVar) DA method as described in Kwon et al. (2018) and Song et al. (2017). KIM's 4DEnVar DA system consists of deterministic and stochastic (ensemble) components whose atmospheric analyses are generated using the KIM VARiational DA (KVAR, Song and Kwon, 2015) and four-dimensional local ensemble transform Kalman filter (LETKF, Shin et al., 2016) schemes, respectively. KIM LETKF independently performs analysis updates by assimilating almost the same atmospheric observations as used in the

358 deterministic component (i.e., KVAR), but the main function of LETKF in the KIM DA
359 system is currently to construct ensemble background error covariance of KVAR (Kwon et
360 al., 2018). The relative contribution of the ensemble background error covariance gradually
361 increases from 45% at the poles to 70% at the equator in the troposphere and then gently
362 decreases above the troposphere. Three-dimensional spatial localizations are implemented
363 using the Gaspari and Cohn Gaussian-like localization function (Gaspari and Cohn, 1999). To
364 obtain an appropriate ensemble spread in LETKF, an additive inflation (Shin et al., 2018) and
365 relaxation-to-prior perturbation (Whitaker and Hamill, 2012) are applied together.
366 In this study, we assimilate both conventional and non-conventional atmospheric data
367 including the Advanced Microwave Sounding Unit-A (AMSU-A), Atmospheric Motion
368 Vectors (AMVs), Microwave Humidity Sounder (MHS), Global Positioning System Radio
369 Occultation (GPS-RO), Infrared Atmosphere Sounding Interferometer (IASI), Advanced
370 Technology Microwave Sounder (ATMS), Cross-track Infrared Sounder (CrIS), and
371 observations obtained from surface, aircraft, and sonde. The KIM Package of Observation
372 Processing (KPOP, Kang et al., 2019) is employed to preprocess (e.g., quality control and
373 bias correction) the observations before assimilation.
374
375 **4.2. Land soil moisture DA**
376 In the KIM-LIS coupled system, land DA is conducted by the LIS-DA subsystem (Figure
377 1) in which various DA schemes are available. The current study applies a 1-dimensional
378 EnKF method (Reichle et al., 2002b) to assimilate satellite soil moisture retrievals (i.e.,
379 ASCAT and SMAP) into the Noah LSM. The EnKF is one of the widely used DA schemes

for nonlinear hydrological applications (e.g., Cho et al., 2023; Crow and Van den Berg, 2010; Draper and Reichle, 2019; Kim et al., 2021a; Kwon et al., 2019, 2021; Reichle et al., 2023; Renzullo et al., 2014; Xu et al., 2021) because of its relatively flexible and computationally efficient nature (Keppenne, 2000).

Within the EnKF-based DA system, model forecasts and analysis updates are performed alternately. That is, the ensemble forecasts of model prognostic state variables are propagated forward in time until observations are available, and the forecasted states are updated in the assimilation step when and where observations exist. The resulting analysis ensemble is then used as the initial condition for the next model forecast. In this study, the control vectors that are directly updated by assimilating the ASCAT and SMAP soil moisture retrievals include the Noah LSM estimates of soil moisture at four soil layers while other related hydrometeorological variables are adjusted through model physics in subsequent model integrations. As we conduct the 1-dimensional EnKF, the soil moisture analysis in a given grid is produced independently of neighboring grids.

The EnKF increments are determined depending on the relative uncertainties (error variances) of model and observation. The model uncertainty (background error covariance) is represented by the ensemble forecast spread (ensemble size of 20), which is obtained at each grid by randomly perturbing the atmospheric variables from KIM including shortwave radiation, longwave radiation, and precipitation, and by additionally (randomly) perturbing the Noah LSM-simulated soil moisture estimates. Shortwave radiation and precipitation are perturbed by applying log-normally distributed multiplicative perturbations with standard deviations of 0.3 and 0.5, respectively, while normally distributed additive perturbations are

applied to longwave radiation (with a standard deviation of 50 W m^{-2}) and the soil moisture (SM) estimates at four soil layers [with standard deviations of 0.01, 0.006, 0.003, and 0.0015 m^3 m^{-3} for SM1 (top layer), SM2, SM3, and SM4 (bottom layer), respectively]. First-order autoregressive temporal correlations and cross-variable correlations are also considered during the perturbation (Table 1), whereas horizontal error correlations are neglected. The perturbation parameters used in this study are determined based on Kumar et al. (2017, 2019) and Reichle et al. (2008), and have also been effectively applied in Jun et al. (2021) and Kwon et al. (2024).

Table 1. Perturbation parameter values used for autoregressive temporal correlation and cross correlations between different variables (SW: shortwave radiation, LW: longwave radiation, P: precipitation, SM1: top layer soil moisture, SM2: second layer soil moisture, SM3: third layer soil moisture, and SM4: bottom layer soil moisture).

Perturbed variables	Time scale of first-order autoregressive temporal correlations (hour)	Cross correlations with perturbations in			
KIM atmospheric forcing		SW	LW		P
SW	24	1.0	−0.5		−0.8
LW	24	−0.5	1.0		0.5
P	24	−0.8	0.5		1.0
Noah LSM soil moisture		SM1	SM2	SM3	SM4
SM1	12	1.0	0.6	0.4	0.2
SM2	12	0.6	1.0	0.6	0.4
SM3	12	0.4	0.6	1.0	0.6
SM4	12	0.2	0.4	0.6	1.0

The spatially and temporally constant observation error standard deviations of 10% and 0.02 m^3 m^{-3} are applied for ASCAT and SMAP soil moisture retrievals, respectively, based on previous DA studies (e.g., Dorigo et al., 2010; Draper et al., 2012; Ferguson et al., 2020; Kolassa et al., 2017; Kwon et al. 2022, 2024). In the KIM-LIS coupled system, the ASCAT-derived soil wetness index data are scaled into the Noah LSM soil moisture climatology (in m^3 m^{-3}) through the CDF matching (see Section 3.3) to remove the systematic bias between

421 the ASCAT soil moisture and Noah-simulated soil moisture. Correspondingly the 10%
422 ASCAT soil moisture error standard deviation is also locally scaled by the ratio of the Noah
423 LSM and ASCAT soil moisture time series standard deviations following Draper et al. (2012)
424 and Jun et al. (2021). Unlike ASCAT, the SMAP soil moisture data are provided in the same
425 unit as the Noah LSM soil moisture, and only the climatological mean biases between the
426 SMAP soil moisture and modeled soil moisture are corrected during the bias correction
427 procedure (see Section 3.3). Therefore, the observation error standard deviation of SMAP is
428 not scaled in this study.
429 Note that there is a mismatch in the surface soil layer depth between the soil moisture
430 observations (i.e., 0–2 cm for ASCAT and 0–5 cm for SMAP) and Noah LSM (i.e., 0–10 cm).
431 However, Shellito et al. (2016, 2018) and Nair and Indu (2019) have demonstrated that
432 changing the surface layer depth in the model from 10 cm to 2 cm or 5 cm has only a
433 marginal impact on the simulated soil moisture. Moreover, because we apply the systematic
434 bias correction of the soil moisture retrievals before assimilation, the impact of the surface
435 soil layer depth difference on the DA performance is assumed to be negligible.
436
437 **5. Experiments**
438 Land-atmosphere coupled DA experiments (with a 6-hour cycling frequency) using the
439 active radar (i.e., ASCAT) and passive radiometer (i.e., SMAP) soil moisture retrievals are
440 designed as summarized in Table 2. CTL, a control case serving as a baseline experiment,
441 only assimilates atmospheric observations while an open-loop ensemble simulation of the
442 Noah LSM is performed without soil moisture assimilation. SG_AT and SG_SP are single-

sensor soil moisture DA experiments where the near-surface soil moisture data from individual sensors (ASCAT or SMAP, respectively) are assimilated into the Noah LSM using the 1-dimensional EnKF with an ensemble size of 20. MT_ATSP, a multi-sensor soil moisture DA experiment, jointly assimilates both ASCAT and SMAP soil moisture products to investigate the synergistic impact of assimilating the radar- and radiometer-based soil moisture retrievals together on improving the atmospheric analysis/forecast of the KIM-LIS coupled system. As explained in Section 3.3, the CDF matching and anomaly correction methods are applied for bias correction of the ASCAT and SMAP soil moisture retrievals, respectively, in the single- and multi-sensor soil moisture DA experiments. Atmospheric DA is performed identically in all experiments.

Table 2. Summary of land-atmosphere coupled data assimilation (DA) experiments conducted in this study (SM: soil moisture; see Appendix A for additional abbreviations).

	CTL*	**SG_AT**	**SG_SP***	**MT_ATSP**
Land				
SM DA	X	O	O	O
SM data	-	ASCAT	SMAP	ASCAT + SMAP
SM bias correction method	-	CDF matching	anomaly correction	CDF matching (ASCAT); anomaly correction (SMAP)
SM DA scheme	-	EnKF	EnKF	EnKF
LSM	Noah LSM v2.7.1 (KIM-LSM) and v3.3 (LIS-LSM)			
LSM horizontal resolution	25 km			
LSM ensemble size	20			
Atmosphere				
KIM	KIM v3.9			
KIM horizontal resolution	deterministic component (25 km); ensemble component (50 km)			
Atmospheric DA scheme	deterministic component (4DEnVar); ensemble component (LETKF)			
KIM ensemble size	50			
Experimental period	April 1 to July 31, 2022 (DA spin-up: March 1 to 31, 2022)			

*Note that CTL and SG_SP are the same experiments as those presented in Kwon et al. (2024).

This study uses the same model setup and experimental period as in Kwon et al. (2024). We use the Shuttle Radar Topography Mission (SRTM) elevation (Farr et al., 2007), MODIS-IGBP land cover (Friedl et al., 2002), National Centers for Environmental Prediction (NCEP) green vegetation fraction and surface albedo, and the blended State Soil Geographic (STATSGO, Miller and White, 1998)/Food and Agriculture Organization (FAO) soil texture (Reynolds et al., 2000) as land inputs for the Noah LSM. The LSM and KIM deterministic component are run over the global domain at a horizontal resolution of 25 km while the KIM ensemble component is run at a 50 km horizontal resolution due to its high computational cost in the 6-hourly cycling experiments. All 6-hourly cycling experiments are conducted from March to July 2022 while the first month is excluded from evaluation as it is used as the assimilation spin-up (burn-in) period. To obtain LSM initial conditions at the beginning of the experiments (i.e., March 1, 2022), an offline spin-up of the Noah LSM is first run from 2008 to April 2020 forced by the meteorological forcing fields from the Global Land Data Assimilation System (GLDAS, Rodell et al., 2004), followed by additional spin-up until March 1, 2022 using the KIM atmospheric forcing, which is available only from May 2020 for the LSM offline simulation. The KIM atmospheric model is initialized by the fifth generation of the European Centre for Medium-Range Weather Forecasts (ECMWF) atmospheric reanalysis (ERA5, Hersbach et al., 2020). In addition to the cycling runs in each experimental case, 5-day forecasts are performed every 00 UTC and 12 UTC cycle after being initialized by the land and atmospheric analyses from DA.

6. Performance evaluation

Due to the difficulty in acquiring a global ground truth reference dataset, we perform global-scale performance evaluations of the soil moisture DA for different hydrometeorological variables using datasets from various sources such as satellite-based observations and analysis fields from different systems. The four experiments (i.e., CTL, SG_AT, SG_SP, and MT_ATSP) listed in Table 2 are assessed in terms of generating the soil moisture analysis, specific humidity and air temperature analyses/forecasts, and precipitation forecasts. Methodologies and datasets employed in this study for the evaluation are described below.

6.1. Soil moisture

A triple collocation analysis (TCA, Stoffelen, 1998; Scipal et al., 2008), a statistical random error estimation method, is applied to evaluate the global soil moisture analysis from the soil moisture DA experiments. TCA has been initially proposed by Stoffelen (1998) to quantify the error of near-surface ocean wind speed estimates, and it is now one of the most commonly used method for estimating uncertainties in satellite-based soil moisture retrievals (e.g., Dorigo et al., 2010; Gruber et al., 2016; Kim et al., 2021b, 2023; Scipal et al., 2008) or for evaluating large-scale soil moisture simulations of computational models (e.g., Kim et al., 2021a; Kwon et al., 2024; Nair and Indu, 2019; Renzullo et al., 2014) due to no requirement of reliable ground truth reference data that is hard to be obtained at large scales.

499 The TCA approach is based on the assumption of a linear relationship between
500 hypothetical true soil moisture and individual soil moisture estimates as expressed in
501 Equation (1):
502
503 $$\theta_k = \alpha_k + \beta_k \theta_{true} + \varepsilon_k \quad (1)$$
504
505 where θ_k is independent collocated soil moisture datasets (i.e., triplet components, $k \in$ [x, y,
506 z]); α_k and β_k are additive and multiplicative systematic biases of θ_k, respectively, with
507 respect to the unknown hypothetical true soil moisture signal (θ_{true}); and ε_k represents the
508 additive random noise in each soil moisture data (θ_k). The random error (noise) variance ($\sigma^2_{\varepsilon_k}$)
509 of three collocated soil moisture triplets [Equations (2) to (4)] can be derived from variance
510 and covariance equations by introducing additional assumptions, i.e., error orthogonality
511 (independence between the random error of the soil moisture datasets and the unknown soil
512 moisture truth) and zero error-cross correlation (independence of the random errors between
513 the soil moisture datasets) (Gruber et al., 2016).
514
515 $$\sigma^2_{\varepsilon_x} = \sigma^2_x - \frac{\sigma_{xy}\sigma_{xz}}{\sigma_{yz}} \quad (2)$$
516
517 $$\sigma^2_{\varepsilon_y} = \sigma^2_y - \frac{\sigma_{yx}\sigma_{yz}}{\sigma_{xz}} \quad (3)$$
518
519 $$\sigma^2_{\varepsilon_z} = \sigma^2_z - \frac{\sigma_{zx}\sigma_{zy}}{\sigma_{xy}} \quad (4)$$

where σ_k^2 and $\sigma_{\varepsilon_k}^2$ ($k \in$ [x, y, z]) are the variance and random error variance, respectively, of each soil moisture data; and σ_{xy}, σ_{xz}, and σ_{yz} are the covariances of two soil moisture triplet components. In this study, the fractional mean-square error ($fMSE_k$, Draper et al., 2013), ranging from 0 (free-of-noise soil moisture data) to 1 (no meaningful soil moisture signal), is computed using Equation (5). This metric is employed as a TCA-based global soil moisture evaluation measure, following procedures implemented by Kim et al. (2020 and 2021a) and Kwon et al. (2024).

$$fMSE_k = \frac{\sigma_{\varepsilon_k}^2}{\sigma_k^2} \quad (5)$$

In order to meet the zero error-cross correlation assumption, we select two independent satellite-based soil moisture products, i.e., ASCAT and Advanced Microwave Scanning Radiometer 2 (AMSR2) [or Soil Moisture and Ocean Salinity (SMOS)], derived from different microwave sensors using different retrieval algorithms for the first and second soil moisture triplet components while the soil moisture simulations from the experiments (CTL, SG_AT, and SG_SP) are used for the third triplet component (Table 3). Due to the TCA assumptions, it is hard to compose the same reference frame for all experimental cases, especially for the multi-sensor soil moisture DA experiment. Therefore, for a fair comparison, we only evaluate the relative improvement in the soil moisture estimates by comparing fMSE of the single-sensor soil moisture DA with fMSE of CTL that are computed using the same first and second triplet components (i.e., satellite soil moisture retrievals that are not

assimilated in the soil moisture DA experiment) as shown in Table 3. The effects of the multi-sensor soil moisture DA (MT_ATSP) are assessed only for atmospheric variables (see Sections 6.2 and 6.3).

Table 3. Triple collocation analysis (TCA) triplet composition to quantify the relative improvement in the soil moisture estimates by soil moisture data assimilation (DA) as compared to CTL. The CTL soil moisture estimates are also evaluated using the same satellite-based reference soil moisture products as used for each single-sensor soil moisture DA experiment (EXP: SG_AT and SG_SP).

Experiments	Triplets for EXP	Triplets for CTL
SG_AT	AMSR2, SMOS, SG_AT	AMSR2, SMOS, CTL
SG_SP	AMSR2, ASCAT, SG_SP	AMSR2, ASCAT, CTL

The ASCAT, SMOS, and AMSR2 soil moisture data used in TCA are the 12.5-km ASCAT soil moisture Climate Data Record (CDR) version 7 product (H119 and extended H120) based on the TU-Wien change detection algorithm (Wagner et al., 2013), the SMOS-INRA-CESBIO (SMOS-IC) version 2 product, and the AMSR2 X-band Land Parameter Retrieval Model (LPRM) product, respectively. The original datasets are preprocessed by conducting quality control based on quality flags provided in each data product, and spatial resampling using the nearest neighbor distance method to match the spatial resolution of the datasets with that of the LSM outputs (i.e., 25-km latitude-longitude grids). Due to the different local overpass time between the satellite soil moisture products [i.e., 09:30 am/pm LST for ASCAT, 01:30 am/pm LST for ASMR2, and 06:00 am/pm LST for SMOS], the UTC-based Noah-LSM outputs at 04:00 am/pm LST and 11 am/pm LST are extracted for TCA that uses AMSR2/SMOS/SG_AT(or CTL) and AMSR2/ASCAT/SG_SP(or CTL), respectively. We select model outputs at the approximate midpoint time (e.g., 04:00) between

564 the overpass times of two other satellite-based soil moisture triplet components (e.g., 01:30
565 AMSR2 and 06:00 SMOS) for a fair comparison. While some errors may still arise due to
566 sampling-time mismatches between the triplet components, we assume these errors are
567 acceptable since the same sampling time was applied to both CTL and DA experimental
568 outputs to evaluate their relative performance. Please refer to Kwon et al. (2024) and Kim et
569 al. (2023) for more detailed procedures.
570
571 **6.2. Specific humidity and air temperature**
572 Evaluations of the specific humidity and air temperature analyses/forecasts are performed
573 using the ECMWF Integrated Forecasting System (IFS) analysis (ECMWF, 2017) as
574 reference data. The IFS components have undergone continuous evolution since 1979,
575 leading to a steady enhancement in the precision of the IFS analyses and forecasts (Ben
576 Bouallègue et al., 2024). Extensive studies have used the ECMWF-IFS analysis for various
577 purposes such as an atmospheric forcing to drive offline models (e.g., Manco et al., 2023;
578 Ricker et al., 2024), initial and boundary conditions for other forecasting systems (e.g.,
579 Federico et al., 2024; Sacchetti et al., 2024; Torcasio et al., 2023), and a reference data to
580 evaluate modeling systems (e.g., Ben Bouallègue et al., 2024; Kwon et al., 2024; Lee et al.,
581 2020; Polichtchouk et al., 2023; Reichle et al., 2023). The root mean square difference
582 (RMSD) between the atmospheric variables (i.e., specific humidity and air temperature) from
583 each experiment and those from the IFS analysis is computed.
584
585

6.3. Precipitation

Local variations in soil moisture modify boundary-layer heat and moisture fluxes, thereby altering water–energy budgets and influencing convective triggering (Findell and Eltahir, 2003; Pal and Eltahir, 2003) and subsequently influence large-scale dynamics (Cook et al., 2006; Pal and Eltahir, 2003), both of which play key roles in determining precipitation processes. A number of studies have investigated the complex interaction mechanisms between soil moisture and precipitation, referred to as the 'soil moisture-precipitation feedback', using observational analyses (e.g., Catalano et al., 2016; Yang et al., 2018) and computational modeling systems (e.g., Beljaars et al., 1996; Bosilovich and Sun, 1999; Hohenegger et al., 2009; Lin et al., 2023; Pal and Eltahir, 2003). Although these studies generally agree on a predominant positive feedback, the sign and strength vary depending on modeling systems and spatiotemporal scales (Hohenegger et al., 2009; Lin et al., 2023). Differences in the sign of soil moisture-precipitation feedback can be attributed to the complexity of representing the soil moisture-evapotranspiration relationship (Yang et al., 2018) and convective development (Hohenegger et al., 2009). Considerable debate and uncertainty remain regarding the physical mechanisms determining the sign of the feedback (Hohenegger et al., 2009). Nevertheless, there is no doubt that soil moisture and precipitation are reciprocally linked, implying that better characterization of soil moisture conditions through soil moisture DA can enhance precipitation forecasts in land-atmosphere coupled systems.

We assess the impact of soil moisture DA on precipitation forecast skill using a well-established metrics such as the frequency bias (FB) and equitable threat score (ETS) based on

608 recommendations by the World Meteorological Organization (WMO, 2008). Calculations of
609 the FB and ETS metrics are based on a 2 × 2 contingency table (Table 4), which consists of
610 *Hits*, *Misses*, *FalseAlarms*, and *CorrectNegatives*. Gauge-based global daily precipitation
611 analyses from the National Oceanic and Atmospheric Administration (NOAA) Climate
612 Prediction Center (CPC) (Chen et al., 2008; Xie et al., 2007) are used as reference data for
613 precipitation evaluation.
614
615 **Table 4.** Contingency table for computing precipitation forecast evaluation metrics

		Observation (reference data)	
		Yes	**No**
Forecast (model data)	**Yes**	*Hits*	*FalseAlarms*
	No	*Misses*	*CorrectNegatives*

616
617 FB [Equation (6)] assesses the ratio of the frequency of precipitation occurrence in the
618 forecast to that in the observation:
619 $$FB = \frac{Hits+FalseAlarms}{Hits+Misses} \quad (6)$$
620
621 where *Hits*, *FalseAlarms*, and *Misses* are the number of model grid points with correct
622 forecasts, false alarms, and missed forecasts of precipitation occurrence, respectively. The FB
623 metric ranges from zero to infinity where the ideal FB score is 1.0, indicating that the number
624 of the forecasted precipitation events is the same as that of the observed events. Note that FB
625 does not consider the timing of precipitation events.

626 ETS [Equation (7)] quantifies the fraction of the forecasted or observed precipitation
627 events that are captured correctly after excluding random hits ($Hits_{rnd}$), which is the number
628 of correct forecasts by random chance computed using Equation (8):
629
630 $$ETS = \frac{Hits - Hits_{rnd}}{Hits + Misses + FalseAlarms - Hits_{rnd}} \quad (7)$$
631
632 $$Hits_{rnd} = \frac{(Hits + Misses)(Hits + FalseAlarms)}{N} \quad (8)$$
633
634 where *N* is the total number of events defined as $N = Hits + Misses + FalseAlarms +$
635 $CorrectNegatives$. *CorrectNegatives* denotes the number of correct forecasts of no
636 precipitation. The ETS metric ranges from −1/3 to 1, where values below 0 and 1 represent
637 "no skill" and "perfect skill" (no *Misses* or *FalseAlarms*), respectively.
638
639 **7. Results**
640 In this section, we first examine the performance of the KIM-LIS coupled system in
641 producing enhanced global soil moisture estimates when the system is informed by satellite-
642 based soil moisture retrievals from ASCAT and SMAP via assimilation. Next, the impacts of
643 assimilating the ASCAT and SMAP soil moisture data, both individually and simultaneously,
644 on atmospheric analyses and forecasts are assessed. Finally, we evaluate the added skill of the
645 KIM-LIS system in forecasting precipitation when using initialized soil moisture conditions
646 from multi-sensor soil moisture DA.

7.1. Soil moisture analysis

The impact of single-sensor soil moisture assimilation (i.e., SG_AT and SG_SP) on the global soil moisture estimates is evaluated using the TCA method (see Section 6.1). Figure 2 presents the spatial distribution of fMSE obtained from TCA during the experimental period from April to July 2022. Both ASCAT and SMAP are seen to have an overall positive impact on the surface soil moisture estimates of the Noah LSM through assimilation. Compared to the CTL experiment, which does not assimilate soil moisture data, SG_AT and SG_SP reduce the global mean fMSE by 4.0% (Figure 2a) and 10.5% (Figure 2b), respectively. In both single-sensor soil moisture DA cases, obvious improvements in soil moisture are observed in Asia while a decrease in skill is mostly found in the Australian and North American continents where CTL already exhibits a relatively good performance in estimating soil moisture.

Note that we use identical first and second triplet components for DA and CTL (Table 3), replacing only the CTL soil moisture estimates with those from the DA experiments (SG_AT and SG_SP) to assess the relative performance gain from soil moisture DA. This approach (i.e., replacing one triplet member) may alter the fMSE calculation of the other two triplet components and thus influence the comparison results between DA and CTL. However, because the soil moisture estimates from DA and CTL share the same spatial and temporal coverage and climatology, as they are generated from the identical modeling system, the impact of replacing the model-based triplet member is negligible, as shown in Figure S1. Therefore, the fMSE comparison results (Figure 2) can be considered reliable.

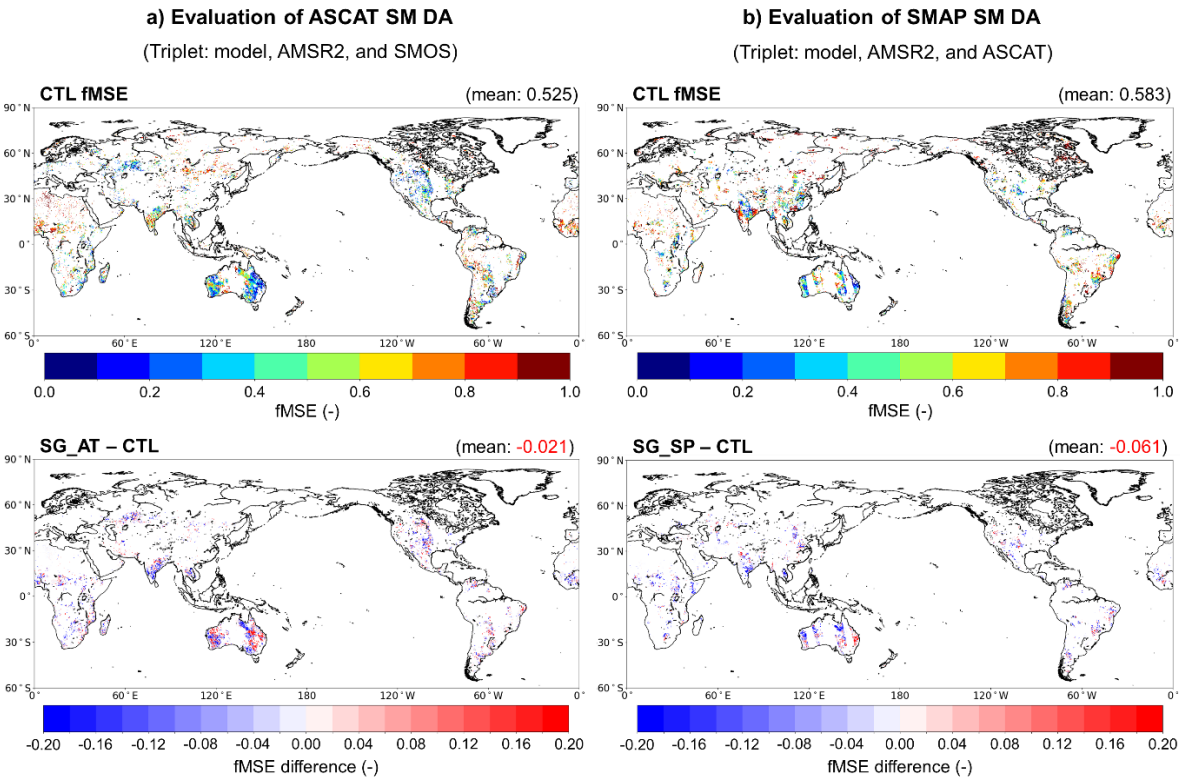

Figure 2. Global maps of the soil moisture triple collocation analysis (TCA) results for (a) ASCAT (i.e., SG_AT) and (b) SMAP soil moisture data assimilation (i.e., SG_SP). Upper panels show the fractional mean-square error (fMSE) of CTL soil moisture at 04:00 am/pm local solar time (LST) (left panel) and 11:00 am/pm LST (right panel), respectively. Lower panels show the soil moisture fMSE difference between SG_AT and CTL (left panel) and between SG_SP and CTL (right panel) where the negative fMSE difference indicates the improved soil moisture estimates by ASCAT and SMAP soil moisture DA, respectively.

Because land surface characteristics affect the soil moisture skill of models and observations (Draper et al., 2012), the TCA results are also plotted for the MODIS-IGBP land cover types. Figure 3 shows that for all land cover types, both SG_AT and SG_SP enhance the skill of the modeled soil moisture relative to CTL in terms of the median fMSE, with SG_SP achieving greater skill gains. The soil moisture estimates are significantly improved by SG_AT for evergreen broadleaf forests and croplands, and by SG_SP for deciduous needleleaf forests, deciduous broadleaf forests, mixed forests, open shrublands, woody

savannas, savannas, grasslands, croplands, and barren or sparsely vegetated land cover types. In both SG_AT and SG_SP experiments, the highest skill improvements, in terms of the median fMSE, are observed for croplands. This implies that the land DA system effectively utilizes soil moisture signals related to agricultural practices from satellite observations, especially in the case of SMAP soil moisture DA (SG_SP), which employs the anomaly-based bias correction approach.

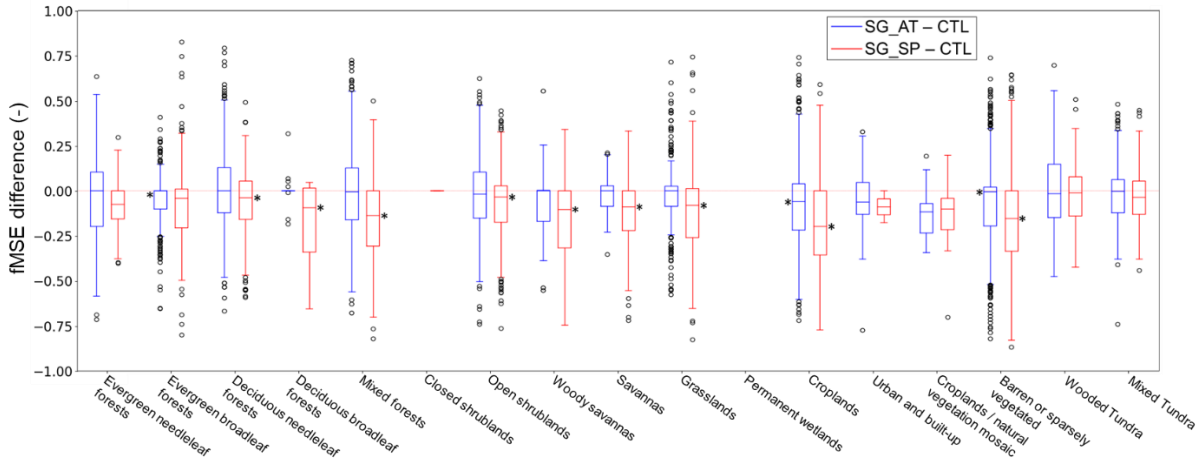

Figure 3. Differences in the soil moisture fractional mean-square error (fMSE) between the single-sensor soil moisture data assimilation (i.e., SG_AT and SG_SP) and control [without soil moisture data assimilation (DA); i.e., CTL] experiments depending on land cover types. A dominant land cover type in each model grid is obtained from the MODIS-IGBP land cover classifications (Friedl et al., 2002). The asterisk symbol (*) indicates statistical significance at $p < 0.05$. Negative values represent the improved soil moisture estimates by soil moisture DA. Results are not plotted for closed shrublands and permanent wetlands because of missing triplet data.

Figures 2 and 3 indicate that SMAP DA shows higher skill than ASCAT DA for the soil moisture analysis. The superior performance of SMAP over ASCAT within a land DA system is also reported in Seo et al. (2021) where SMAP and ASCAT soil moisture DA results are evaluated against *in situ* measurements in the continental United States. These

706 results can be supported by the fact that L-band brightness temperature measurements have
707 higher sensitivity to soil moisture variations than C-band backscatter measurements (Kolassa
708 et al., 2017), and thus the SMAP soil moisture retrievals have better accuracy (Al-Yaari et al.,
709 2019; Kumar et al., 2018). However, note that in this study, a direct comparison of the global
710 soil moisture analysis between SG_AT and SG_SP is not made because the model soil
711 moisture outputs used in TCA are extracted at different LST—specifically, 04:00 am/pm for
712 SG_AT and 11:00 am/pm for SG_SP—due to the different local overpass times of the
713 satellite soil moisture data used for TCA-based assessment (see Section 6.1).
714 As shown in Figure 2, soil moisture performance gains and losses by each single-sensor
715 soil moisture DA are locally dependent. Thus, some previous studies (e.g., Draper et al., 2012;
716 Kolassa et al., 2017) have shown that simultaneously assimilating soil moisture retrievals
717 from both passive and active sensors achieves higher model soil moisture accuracy than
718 assimilating a single product. However, because soil moisture triplets that fully satisfy the
719 TCA assumptions (see Section 6.1) are difficult to obtain over the global domain for the
720 multi-sensor soil moisture DA experiment, the combined effects of ASCAT and SMAP DA
721 are discussed only in terms of atmospheric variables, which are the ultimate objective of this
722 study, in the subsequent sections.
723
724 **7.2. Analysis and forecast of specific humidity and air temperature**
725 Domain-averaged RMSD differences (i.e., $RMSD_{EXP}$ minus $RMSD_{CTL}$) in the specific
726 humidity analysis (Figures 4a to 4c) and air temperature analysis (Figures 4d to 4f) are
727 evaluated across atmospheric levels and over time. Compared to CTL (without soil moisture

728 DA), ASCAT DA (i.e., SG_AT) has more beneficial impacts on the air temperature analysis
729 (Figure 4d) while SMAP DA (i.e., SG_SP) has more beneficial impacts on the specific
730 humidity analysis (Figure 4b). Figures 4c and 4f show that the simultaneous assimilation of
731 ASCAT and SMAP soil moisture retrievals (i.e., MT_ATSP) improves the analysis of both
732 atmospheric variables relative to CTL. Notably, degradations in the specific humidity and air
733 temperature analyses by SG_AT and SG_SP, respectively, are compensated by additionally
734 assimilating other soil moisture products.

735 Figure 5 more clearly demonstrates that multi-sensor soil moisture DA enhances the
736 performance of the specific humidity (Figure 5a) and air temperature analyses (Figure 5d)
737 compared to the single-sensor soil moisture DA cases (i.e., SG_AT and SG_SP, respectively).
738 Although MT_ATSP exhibits somewhat reduced performance in the air temperature (Figure
739 5c) and specific humidity analyses (Figure 5b) compared to SG_AT and SG_SP, respectively,
740 it achieves a more balanced improvement, meaning that neither variable is degraded while
741 both show moderate gains compared to CTL, by assimilating radar- and radiometer-based
742 soil moisture data together.

743 Tables 5 and 6 summarize the domain-averaged RMSD differences between the soil
744 moisture DA experiments and CTL for the analyses and forecasts of 2-m atmospheric
745 variables (i.e., specific humidity and air temperature) from the 00 UTC cycle (Table 5) and
746 the 12 UTC cycle (Table 6). In the global domain, SG_SP generally achieves better domain-
747 averaged analysis and forecast skills for both 2-m atmospheric variables compared to SG_AT
748 (Tables 5 and 6), except for the 2-m air temperature forecast of the 12 UTC cycle, where
749 SG_AT performs slightly better (Table 6). During the experimental period, all soil moisture

DA cases are more effective in improving the 2-m air temperature analysis and forecast than those of specific humidity, especially for the 00 UTC cycle. Overall, they perform better in the Northern Hemisphere than in the Southern Hemisphere (Tables 5 and 6), although they achieve greater 2-m air temperature forecast skill during the 00 UTC cycle in the Southern Hemisphere (Table 5). The lower analysis and forecast skills of soil moisture DA in the Southern Hemisphere can be attributed to the use of spatially and temporally constant observations errors (see Section 4.2), which do not adequately reflect the relatively higher uncertainties in winter-period soil moisture data.

For the 2-m specific humidity estimates, the assimilation of SMAP soil moisture retrievals alone (SG_SP) achieves the best domain-averaged performance (Tables 5 and 6). MT_ATSP reduces RMSD compared to SG_AT by additionally assimilating the SMAP soil moisture data, but it exhibits relatively lower skill in specific humidity than SG_SP. However, in Europe and tropical regions, MT_ATSP provides improved 2-m specific humidity forecasts compared to SG_SP, particularly when both ASCAT and SMAP have a positive impact. The synergistic impacts of the combined assimilation of ASCAT and SMAP are evident in the 2-m air temperature analysis and forecast of the 00 UTC cycle (Table 5).

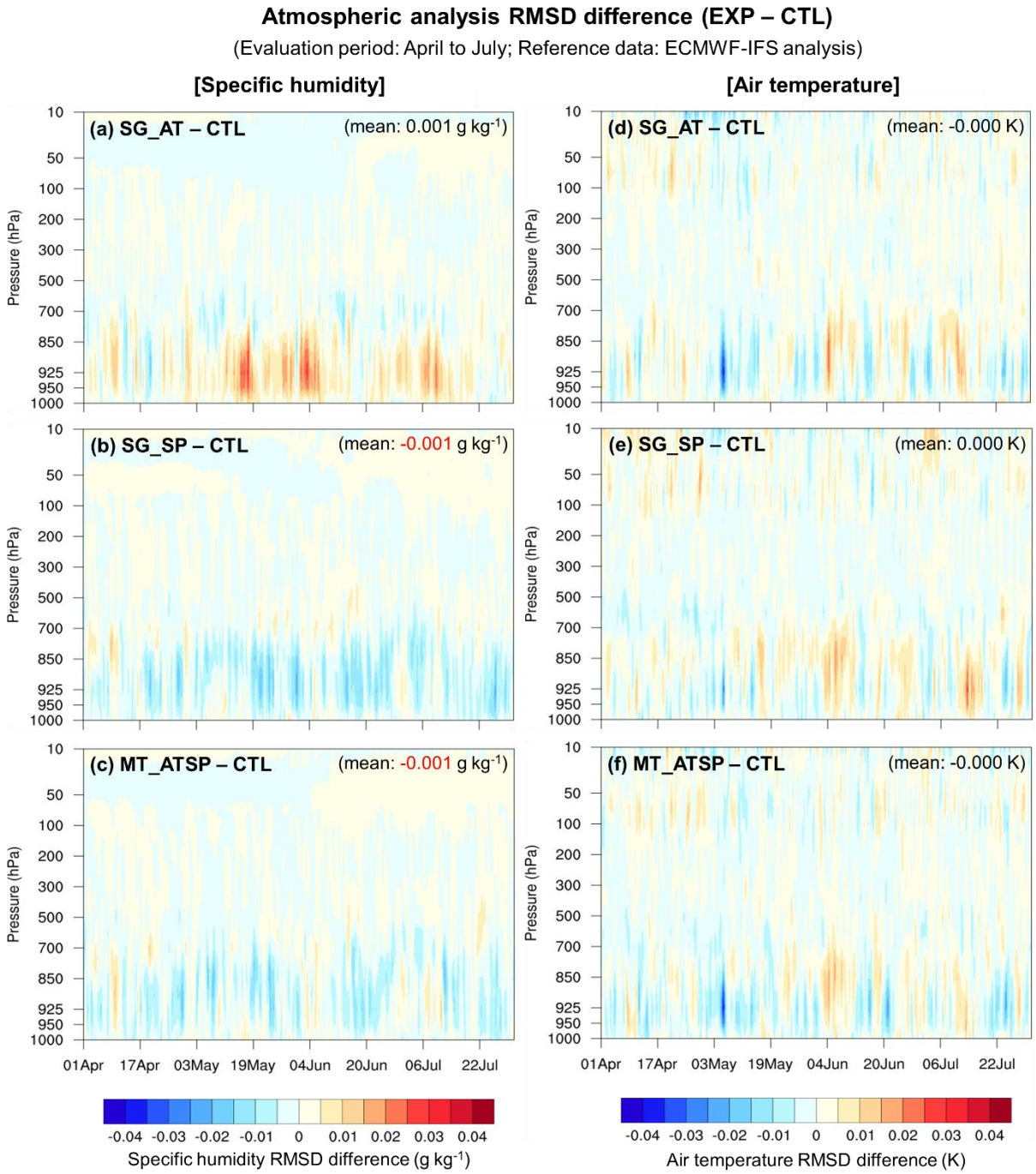

Figure 4. Vertical profile time series of RMSD differences in the specific humidity analysis (left column) and air temperature analysis (right column) between the soil moisture data assimilation (DA) and CTL experiments. The RMSD is calculated using the ECMWF-IFS analysis as reference data. Negative RMSD differences indicate improved estimates of the atmospheric variables by assimilating the soil moisture retrievals.

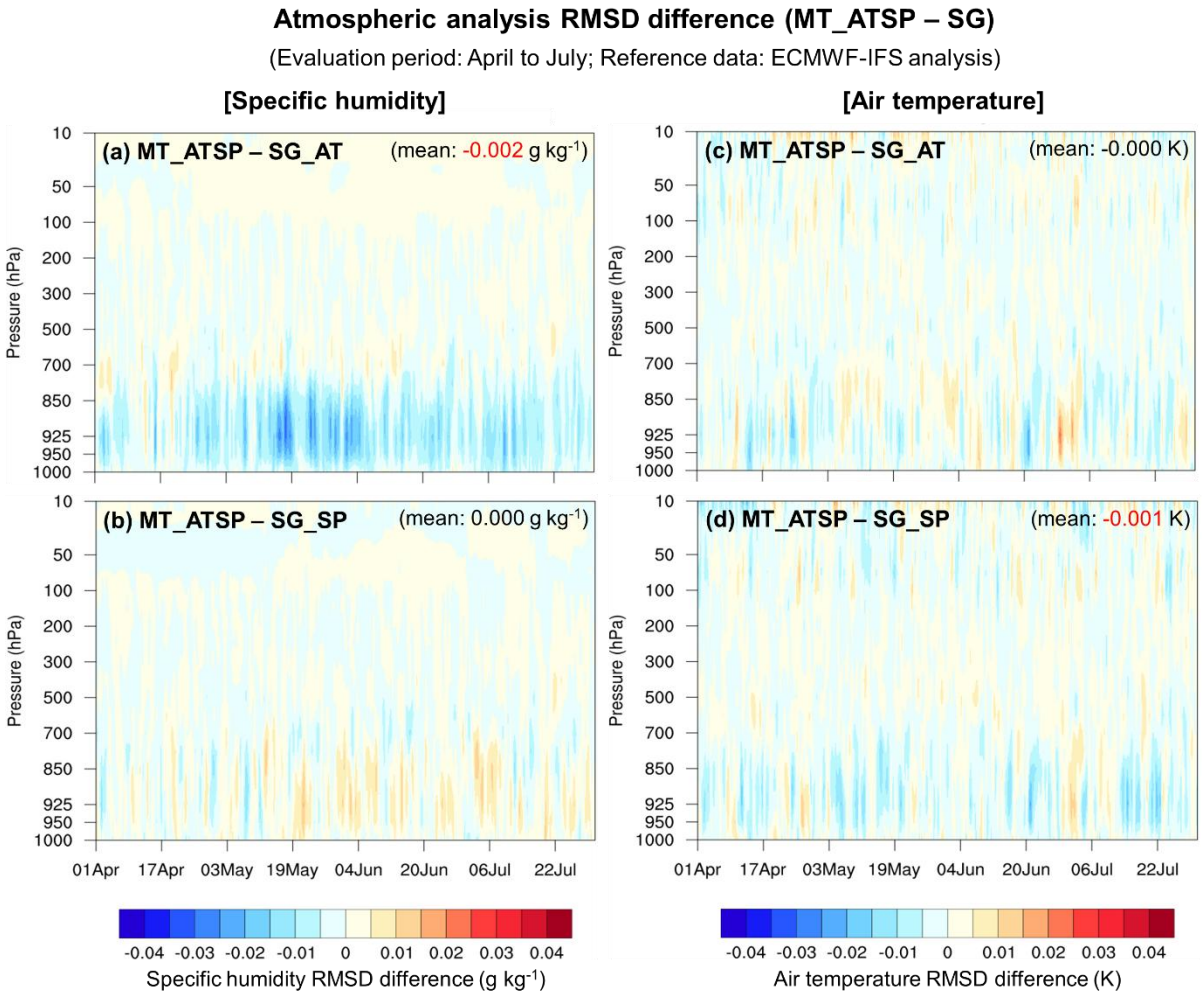

Figure 5. Vertical profile time series of RMSD differences in the specific humidity analysis (left column) and air temperature analysis (right column) between the multi-sensor soil moisture data assimilation (DA) (MT_ATSP) and single- sensor soil moisture DA [SG_AT (a and c) and SG_SP (b and d)] experiments. The RMSD is calculated using the ECMWF-IFS analysis as reference data. Negative RMSD differences indicate improved estimates of the atmospheric variables by additionally assimilating the SMAP or ASCAT soil moisture retrievals.

Table 5. Domain-averaged RMSD differences (ΔRMSD = $RMSD_{EXP}$ – $RMSD_{CTL}$) for the 2-m specific humidity and air temperature analyses and (5-day) forecasts across six domains [i.e., global domain (GLOB), Northern Hemisphere (NH), Southern Hemisphere (SH), Asia (ASIA), Europe (EU), and tropical area (TROP)]. The RMSD is calculated for the 00 UTC cycle from April to July 2022 (whole experimental period) using the ECMWF-IFS analysis as reference data. Negative ΔRMSD indicates improved estimates of the atmospheric variables by assimilating the soil moisture retrievals.

April to July 2022 (00 UTC)	**2-m specific humidity ΔRMSD (EXP – CTL) [g kg^{-1}]**																	
	Analysis			**Forecast**														
				1-day lead time			**2-day lead time**			**3-day lead time**			**4-day lead time**			**5-day lead time**		
Domain	**SG_ AT**	**SG_ SP**	**MT_ ATSP**	**SG_ AT**	**SG_ SP**	**MT_ ATSP**	**SG_ AT**	**SG_ SP**	**MT_ ATSP**	**SG_ AT**	**SG_ SP**	**MT_ ATSP**	**SG_ AT**	**SG_ SP**	**MT_ ATSP**	**SG_ AT**	**SG_ SP**	**MT_ ATSP**
GLOB	0.011	**-0.001**	0.001	0.012	0.001	0.002	0.014	0.004	0.005	0.013	0.004	0.004	0.014	0.004	0.006	0.017	0.004	0.010
NH	0.005	**-0.006**	**-0.005**	0.005	**-0.004**	**-0.004**	0.006	**-0.002**	**-0.001**	0.006	**-0.002**	**-0.001**	0.005	**-0.004**	0.000	0.009	**-0.005**	0.001
SH	0.046	0.025	0.040	0.029	0.011	0.016	0.026	0.010	0.012	0.017	0.006	0.007	0.018	0.007	0.009	0.022	0.016	0.025
ASIA	0.004	**-0.004**	**-0.002**	0.003	**-0.001**	0.000	0.006	0.002	0.003	0.008	0.004	0.004	0.009	0.003	0.006	0.009	0.006	0.010
EU	0.016	**-0.001**	0.003	0.012	**-0.002**	**-0.004**	0.010	**-0.000**	**-0.005**	0.004	**-0.001**	**-0.006**	0.002	0.006	0.000	0.002	0.003	0.001
TROP	0.008	**-0.001**	**-0.004**	0.016	0.005	0.005	0.021	0.011	0.010	0.022	0.012	0.011	0.023	0.013	0.013	0.025	0.014	0.017
	2-m air temperature ΔRMSD (EXP – CTL) [K]																	
	Analysis			**Forecast**														
				1-day lead time			**2-day lead time**			**3-day lead time**			**4-day lead time**			**5-day lead time**		
Domain	**SG_ AT**	**SG_ SP**	**MT_ ATSP**	**SG_ AT**	**SG_ SP**	**MT_ ATSP**	**SG_ AT**	**SG_ SP**	**MT_ ATSP**	**SG_ AT**	**SG_ SP**	**MT_ ATSP**	**SG_ AT**	**SG_ SP**	**MT_ ATSP**	**SG_ AT**	**SG_ SP**	**MT_ ATSP**
GLOB	0.001	0.000	**-0.003**	**-0.000**	**-0.014**	**-0.013**	0.001	**-0.013**	**-0.011**	0.001	**-0.011**	**-0.010**	0.003	**-0.010**	**-0.008**	0.005	**-0.009**	**-0.003**
NH	0.001	**-0.008**	**-0.007**	0.002	**-0.005**	**-0.005**	0.007	0.002	0.002	0.010	0.006	0.006	0.013	0.009	0.011	0.015	0.008	0.017
SH	0.016	0.002	**-0.003**	0.006	**-0.012**	**-0.009**	**-0.006**	**-0.027**	**-0.022**	**-0.016**	**-0.028**	**-0.028**	**-0.019**	**-0.033**	**-0.029**	**-0.012**	**-0.021**	**-0.024**
ASIA	**-0.000**	**-0.007**	**-0.003**	**-0.001**	**-0.009**	**-0.025**	**-0.003**	**-0.009**	**-0.029**	**-0.003**	**-0.007**	**-0.029**	0.002	**-0.003**	**-0.020**	0.005	**-0.009**	**-0.015**
EU	**-0.005**	**-0.011**	**-0.010**	**-0.009**	**-0.033**	**-0.027**	**-0.001**	**-0.027**	**-0.019**	**-0.000**	**-0.026**	**-0.019**	**-0.003**	**-0.026**	**-0.019**	**-0.012**	**-0.038**	**-0.022**
TROP	**-0.005**	0.012	0.001	**-0.005**	**-0.027**	**-0.027**	**-0.006**	**-0.030**	**-0.028**	**-0.008**	**-0.032**	**-0.029**	**-0.007**	**-0.030**	**-0.029**	**-0.005**	**-0.030**	**-0.027**

Table 6. Same as Table 5 but for the 12 UTC cycle from April to July 2022 (whole experimental period).

April to July 2022 (12 UTC)	2-m specific humidity ΔRMSD (EXP – CTL) [g kg^{-1}]																	
	Analysis			Forecast														
				1-day lead time			2-day lead time			3-day lead time			4-day lead time			5-day lead time		
Domain	**SG_AT**	**SG_SP**	**MT_ATSP**	**SG_AT**	**SG_SP**	**MT_ATSP**	**SG_AT**	**SG_SP**	**MT_ATSP**	**SG_AT**	**SG_SP**	**MT_ATSP**	**SG_AT**	**SG_SP**	**MT_ATSP**	**SG_AT**	**SG_SP**	**MT_ATSP**
GLOB	0.014	0.004	0.006	0.015	0.008	0.010	0.019	0.010	0.014	0.018	0.011	0.015	0.017	0.011	0.016	0.019	0.012	0.019
NH	0.003	**-0.006**	**-0.005**	0.005	**-0.009**	**-0.006**	0.007	**-0.007**	**-0.001**	0.006	**-0.004**	0.002	0.005	**-0.004**	0.002	0.008	**-0.006**	0.003
SH	0.052	0.026	0.036	0.064	0.040	0.050	0.060	0.033	0.045	0.053	0.029	0.041	0.046	0.027	0.042	0.046	0.030	0.046
ASIA	0.006	0.002	0.003	0.007	**-0.002**	0.001	0.011	**-0.000**	0.007	0.009	0.004	0.014	0.009	0.005	0.014	0.011	0.000	0.016
EU	**-0.003**	**-0.007**	**-0.009**	**-0.003**	**-0.005**	**-0.009**	**-0.004**	0.000	**-0.007**	**-0.008**	0.000	**-0.008**	**-0.011**	0.005	**-0.005**	**-0.014**	0.003	0.003
TROP	0.018	0.013	0.013	0.013	0.022	0.019	0.021	0.026	0.026	0.023	0.027	0.026	0.027	0.028	0.029	0.026	0.030	0.033

	2-m air temperature ΔRMSD (EXP – CTL) [K]																	
	Analysis			Forecast														
				1-day lead time			2-day lead time			3-day lead time			4-day lead time			5-day lead time		
Domain	**SG_AT**	**SG_SP**	**MT_ATSP**	**SG_AT**	**SG_SP**	**MT_ATSP**	**SG_AT**	**SG_SP**	**MT_ATSP**	**SG_AT**	**SG_SP**	**MT_ATSP**	**SG_AT**	**SG_SP**	**MT_ATSP**	**SG_AT**	**SG_SP**	**MT_ATSP**
GLOB	**-0.007**	**-0.010**	**-0.015**	0.005	0.018	0.012	0.008	0.018	0.012	0.009	0.019	0.015	0.007	0.017	0.011	0.008	0.018	0.011
NH	0.002	**-0.004**	**-0.007**	**-0.002**	**-0.008**	**-0.008**	**-0.000**	**-0.012**	**-0.009**	**-0.003**	**-0.015**	**-0.011**	**-0.004**	**-0.018**	**-0.018**	**-0.002**	**-0.018**	**-0.017**
SH	0.008	**-0.001**	**-0.004**	0.070	0.037	0.051	0.082	0.045	0.060	0.087	0.050	0.071	0.091	0.060	0.079	0.082	0.056	0.073
ASIA	**-0.006**	**-0.010**	**-0.018**	0.002	**-0.004**	**-0.002**	0.011	**-0.003**	0.004	0.010	**-0.007**	0.004	0.009	**-0.016**	**-0.006**	0.015	**-0.017**	0.001
EU	0.000	**-0.003**	**-0.000**	**-0.021**	**-0.004**	**-0.008**	**-0.026**	**-0.001**	**-0.011**	**-0.031**	0.003	**-0.015**	**-0.032**	0.008	**-0.020**	**-0.033**	0.018	**-0.009**
TROP	**-0.024**	**-0.021**	**-0.029**	**-0.007**	0.049	0.026	**-0.003**	0.053	0.027	**-0.000**	0.058	0.033	**-0.003**	0.054	0.031	**-0.000**	0.058	0.031

Local performance differences in the 2-m atmospheric analysis between the single-sensor soil moisture DA cases are clearly illustrated in Figure 6, which is plotted for the 12 UTC cycle from June to July 2022. SG_AT and SG_SP exhibit opposite impacts on the atmospheric analysis, especially on specific humidity, over India, Eurasia, and Brazil. ASCAT DA (SG_AT) generally leads to the improved analyses of specific humidity and air temperature over India while SMAP DA (SG_SP) performs better in Eurasia (except for India and the southern part of West Asia) and Brazil. These discrepancies in the local performance of 2-m specific humidity between ASCAT and SMAP DA may contribute to the reduced domain-averaged skill of MT_ATSP relative to SG_SP, as shown in Tables 5 and 6. In Africa, SG_AT yields better air temperature analysis than SG_SP, whereas SG_SP outperforms SG_AT in the specific humidity analysis. It can be noted from Figure 6 that, locally, the joint assimilation of the ASCAT and SMAP soil moisture retrievals yields the best estimates of the 2-m atmospheric variables when both soil moisture products have positive impacts.

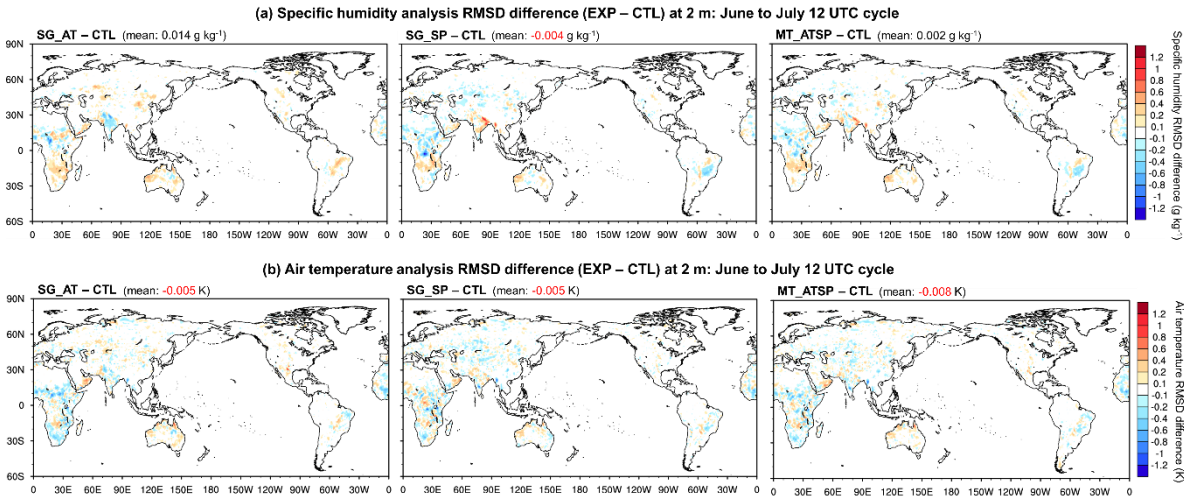

Figure 6. Difference in the 2-m atmospheric analysis RMSD [i.e., specific humidity (upper panels) and air temperature (lower panels)] between the soil moisture data assimilation (DA) and CTL experiments. Evaluation results for the 12 UTC cycle from June to July 2022 (a two-month period) are presented with domain-averaged values in parenthesis. The RMSD is calculated using the ECMWF-IFS analysis as reference data. Negative RMSD differences indicate improved estimates of the atmospheric variables by assimilating the soil moisture retrievals.

7.3. Precipitation

The potential added value of multi-sensor soil moisture DA for precipitation forecasts is assessed using categorical skill score metrics, including the FB and ETS, as detailed in Section 6.3. Daily precipitation rates (mm day^{-1}) are computed from the KIM forecasts at 0-24 h, 24-48 h, and 48-72 h lead times, and compared against reference data using seven conventional thresholds (0.5, 1.0, 5.0, 10.0, 15.0, 20.0, and 25.0 mm day^{-1}). The numbers of model grid points classified as *Hits*, *FalseAlarms*, *Misses*, and *CorrectNegatives* in the contingency table (Table 4) are then counted, and FB and ETS are calculated for six domains (i.e., global domain, Northern Hemisphere, Southern Hemisphere, Asia, Europe, and tropical area). Figure S2 presents the FB and ETS of daily precipitation forecasts from KIM, averaged over the three lead times, for CTL and the three soil moisture DA experiments (SG_AT, SG_SP, and MT_ATSP) during the 00 UTC cycle in July 2022. The corresponding differences ($\Delta\mathrm{FB} = |\mathrm{FB}_{\mathrm{EXP}} - 1| - |\mathrm{FB}_{\mathrm{CTL}} - 1|,\ \Delta\mathrm{ETS} = \mathrm{ETS}_{\mathrm{EXP}} - \mathrm{ETS}_{\mathrm{CTL}}$) are shown in Figure 7.

In the global domain, CTL (without soil moisture DA) tends to overestimate precipitation frequency (FB > 1.0), simulating excessive precipitation events, except for the precipitation threshold of 25.0 mm day^{-1} (Figure S2a). The model significantly overestimates precipitation

838 at the 5.0 mm day^{-1} threshold and exhibits an FB close to 1 for heavier precipitation events
839 (20.0 and 25.0 mm day^{-1}) (Figure S2a), with regional variations (Figures S2b to S2f). Both
840 the smallest FB (close to 1.0) and the largest FB (> 2.5) are observed in the Southern
841 Hemisphere for the lightest (0.5 mm day^{-1}) and heaviest (25.0 mm day^{-1}) precipitation events,
842 respectively (Figure S2c).

843 Unlike FB, ETS is higher (indicating better skill in predicting precipitation events) at
844 lower precipitation thresholds while ETS decreases as the precipitation intensity thresholds
845 increase in the global domain (Figure S2g) and in the Northern Hemisphere (Figure S2h),
846 including Asia (Figure S2j), Europe (Figure S2k), and tropical areas (Figure S2l). In the
847 Southern Hemisphere, CTL shows the highest ETS skill at the precipitation threshold of 10.0
848 mm day^{-1} and the lowest at 1.0 mm day^{-1} (Figure S2i). The different model performance
849 patterns (in both FB and ETS) between the Northern and Southern Hemispheres across the
850 range of precipitation intensity thresholds may be attributed to different weather regimes
851 associated with cyclones and monsoons (Dare and Ebert, 2017), along with additional
852 impacts from seasonal variations.

853 Overall, soil moisture DA improves the prediction of precipitation events (i.e., better ETS;
854 Figure 7g) while its contribution to precipitation frequency (FB) remains neutral (Figure 7a).
855 MT_ATSP demonstrates higher ETS skill than CTL (by up to 1.8%) and single-sensor soil
856 moisture DA (by up to 2.4% and 0.6% relative to SG_AT and SG_SP, respectively) (Figure
857 7g). The impacts of MT_ATSP on the global FB are marginal, showing negligible
858 improvements at the 0.5, 1.0, 5.0, and 25.0 mm day^{-1} thresholds and slight overpredictions at
859 the 10.0, 15.0, and 20.0 mm day^{-1} thresholds (Figure 7a, Figure S2a). Similar soil moisture

DA performance patterns are observed in the Northern Hemisphere (Figures 7b and 7h) and Asia (Figures 7d and 7j). In the Southern Hemisphere, MT_ATSP slightly improves FB for heavy precipitation events (precipitation thresholds ≥ 15.0 mm day^{-1}) while relatively obvious improvements in ETS by MT_ATSP are witnessed at lower thresholds (≤ 1.0 mm day^{-1}) (Figures 7c and 7i). Compared to CTL and SG_AT, multi-sensor soil moisture DA enhances ETS across precipitation thresholds in tropical areas, although it is slightly less effective than SG_SP at thresholds ≤ 5.0 mm day^{-1} (Figure 7l). For FB, MT_ATSP shows improvements over CTL and SG_AT in tropical areas, except at thresholds of 5.0 and 10.0 mm day^{-1}, where SG_SP performs better (Figure 7f). In contrast, MT_ATSP is generally ineffective in Europe (Figures 7e and 7k), except for ETS at precipitation thresholds of 5.0 mm day^{-1} or lower. The overprediction of precipitation in Europe (Figure 7e, Figure S2e), especially for heavy precipitation events (≥ 15.0 mm day^{-1}), may lead to a decrease in ETS (Figure 7k, Figure S2k).

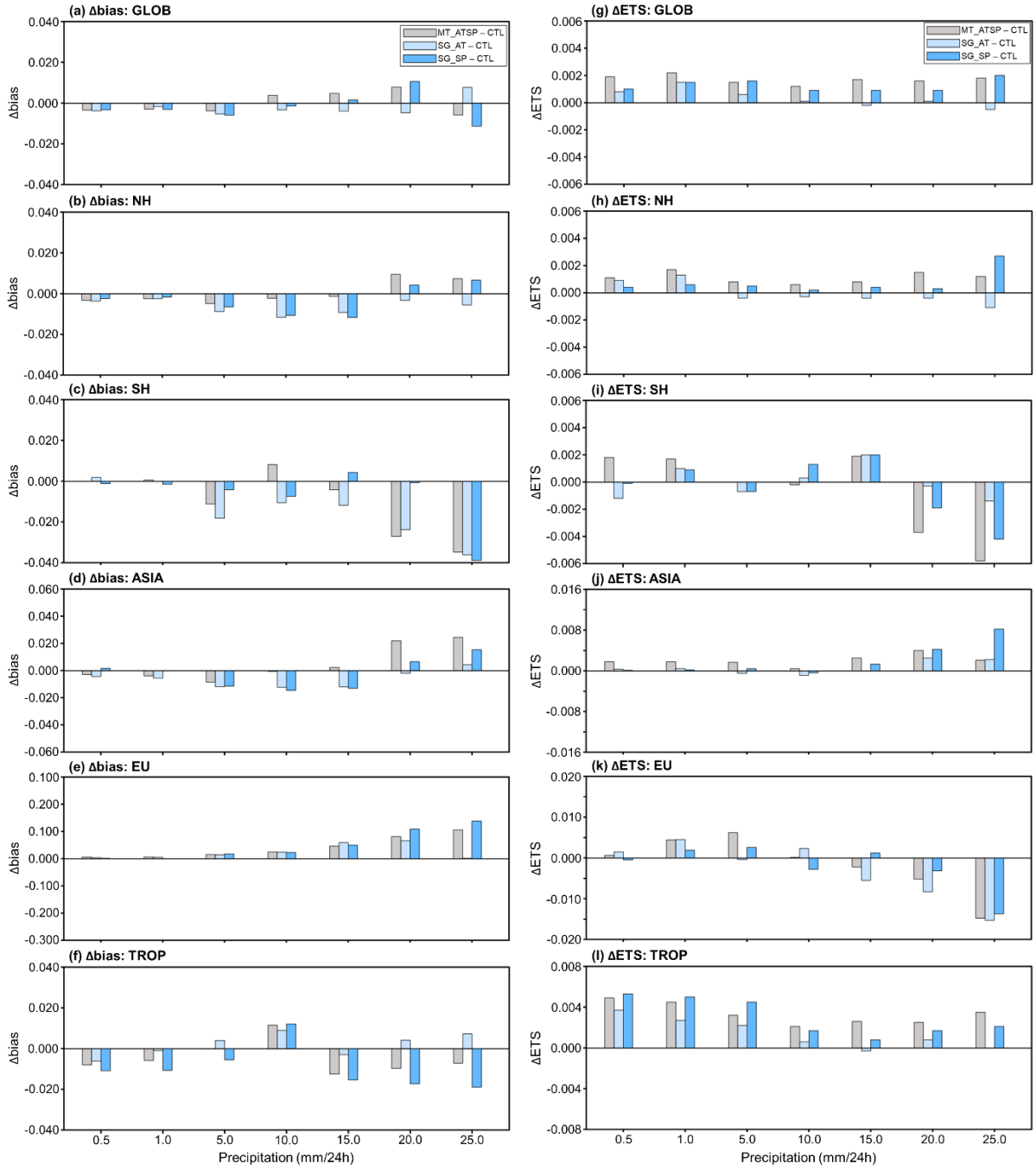

Figure 7. Differences in frequency bias ($\Delta FB = |FB_{EXP} - 1| - |FB_{CTL} - 1|$; a to f) and equitable threat score ($\Delta ETS = ETS_{EXP} - ETS_{CTL}$; g to l) between EXP (MT_ATSP, SG_AT, and SG_SP) and CTL, averaged over 24-72 h precipitation forecasts from the 00 UTC cycle in July 2022, for six domains [i.e., global domain (GLOB; a and g), Northern Hemisphere (NH; b and h), Southern Hemisphere (SH; c and i), Asia (ASIA; d and j), Europe (EU; e and k), and tropical area (TROP; f and l)]. The skill metrics are computed for seven conventional

thresholds (i.e., 0.5, 1.0, 5.0, 10.0, 15.0, 20.0, and 25.0 mm day^{-1}). Negative ΔFB and positive ΔETS values indicate improvements from soil moisture DA.

8. Discussion

8.1. ASCAT data assimilation

The experimental results indicate that SMAP DA slightly outperforms ASCAT DA in enhancing near-surface atmospheric analyses and forecasts. While many factors may affect the overall performance of each experiment, one factor may be related to errors resulting from subsurface scattering, which are not accounted for in the ASCAT soil moisture data used in this study, as discussed by Wagner et al. (2024). The current TU Wien change detection algorithm (Wagner et al., 1999, 2010), used to retrieve soil moisture from ASCAT backscatter observations, is based on the assumption of a positive linear relationship between soil backscatter and wetness. However, Wagner et al. (2024) demonstrated that this assumption fails when coarse fragments (e.g., stones and rocks) or discontinuities exist in the soil profile, as they increase subsurface scattering contributions to total backscatter signals under dry soil conditions. This eventually reverses the relationship between backscatter signals and soil moisture content, deteriorating the quality of soil moisture data retrieved with the current algorithm in many arid and semiarid regions. This phenomenon partly explains why ASCAT DA exhibits better performance in croplands than in barren or sparsely vegetated areas, as shown in Figure 3, which is consistent with results from soil moisture data evaluation studies (e.g., Dorigo et al., 2010).

Soil moisture bias correction methods used to remove systematic discrepancies between observations and models may also influence the ASCAT soil moisture DA performance.

Kumar et al. (2015) and Kwon et al. (2022, 2024) have shown that different bias correction methods can substantially impact soil moisture DA performance. In SMAP DA, soil moisture temporal variability information is directly assimilated (i.e., anomaly correction method). In contrast, ASCAT DA employs the CDF matching method because it does not satisfy the underlying assumption of the anomaly correction method (see Section 3.3). It is a known issue that rescaling-based bias correction, such as CDF matching, causes a significant loss of information (Kumar et al., 2015). Meanwhile, Text S1 and Figures S3-S5 suggest that employing the anomaly correction method in soil moisture DA worsens the atmospheric analysis within land-atmosphere coupled systems when the underlying assumptions of the anomaly correction approach are not met. Rather than relying on CDF matching and anomaly correction methods, a more robust and appropriate bias correction approach is required for improving ASCAT soil moisture DA.

8.2. Soil moisture observation error

The effectiveness of the combined assimilation of multiple soil moisture products from different sources (i.e., radar backscatter and radiometer brightness temperature observations) in enhancing the soil moisture analysis skill has been demonstrated in previous studies (e.g., Blyverket et al., 2019; Draper et al., 2012; Kolassa et al., 2017; Renzullo et al., 2014). Our experimental results also show that, compared to single-sensor soil moisture DA, simultaneous assimilation of the ASCAT and SMAP soil moisture retrievals within the KIM-LIS coupled system has a synergistic impact, improving the analyses and forecasts of atmospheric variables including specific humidity, air temperature, and precipitation.

However, the superiority of individual single-sensor soil moisture retrieval products and their combined performance within the DA system depend on the region and time period (Figure 6). Specifically, locally reduced benefits of SMAP or ASCAT are observed in the multi-sensor soil moisture DA experiment when their performance impacts are opposite (Figure 6). This may be attributed to the use of uniform observation error standard deviations for the soil moisture retrievals across space and time, which is unrealistic and does not adequately reflect the actual and relative retrieval skill of each soil moisture product. Especially, underestimated soil moisture observation errors can degrade the soil moisture and atmospheric analyses by over-relying on less reliable soil moisture data within the DA framework.

One key advantage of simultaneously assimilating individual soil moisture products, rather than a preprocessed multi-sensor-derived soil moisture product, is the flexibility to handle individual soil moisture sensors separately within a single DA system while achieving comparable performance (Kolassa et al., 2017). However, this advantage can be more effectively utilized by accurately specifying the relative errors of the soil moisture retrievals in space and time, enabling the optimal combination of models and diverse soil moisture products.

Several recent studies (e.g., Wu et al., 2021; Kim et al., 2023; Kim et al., 2025) have made efforts to estimate spatially or spatiotemporally distributed errors in satellite-based soil moisture retrievals using TCA-based methods and machine learning algorithms. A map of spatially distributed (but time-invariant) error standard deviations from Kim et al. (2025) [see Figure S6, which is Figure 5a in Kim et al. (2025)] exhibits that the SMAP soil moisture data have errors greater than 0.05 $m^3\ m^{-3}$ in many areas, particularly in forests. Excluding forested

948 areas where soil moisture retrievals are masked out during quality control (see Section 3.4)
949 and thus not assimilated, the error standard deviations of SMAP soil moisture are still above
950 0.02 m^3 m^{-3} (the uniformly applied error value in this study) in some savanna regions of
951 South America and Africa, grasslands in North America, and croplands in South Asia (Figure
952 S6) [see Figure S3c for the land-cover type map generated in this study using the MODIS-
953 IGBP global land-cover classification (Friedl et al., 2002)]. As a result, this leads to
954 degradation in the 2-m specific humidity and air temperature analysis in the regions, as noted
955 in the SMAP soil moisture DA (SG_SP) results shown in Figure 6.
956 Meanwhile, in ASCAT soil moisture DA, the spatially distributed soil moisture
957 observation error standard deviation (m^3 m^{-3}) (Figure 8) is applied after locally rescaling the
958 uniformly specified 10% soil wetness index observation error using the ratio of the standard
959 deviations of modeled and observed soil moisture time series (see Section 4.2). However, the
960 spatial pattern of the ASCAT observation error standard deviations in Figure 8 does not
961 completely match that of the TCA/ML-based ASCAT fMSE computed by Kim et al. (2023)
962 (see their Figure 4f), which was derived using other satellite soil moisture data as triplet
963 components. Notably, the ASCAT errors used in the current study appear to be relatively
964 underestimated in dry areas of Africa and Asia (Figure 8), where the 2-m atmospheric
965 analyses are degraded by ASCAT soil moisture DA (SG_AT in Figure 6).
966

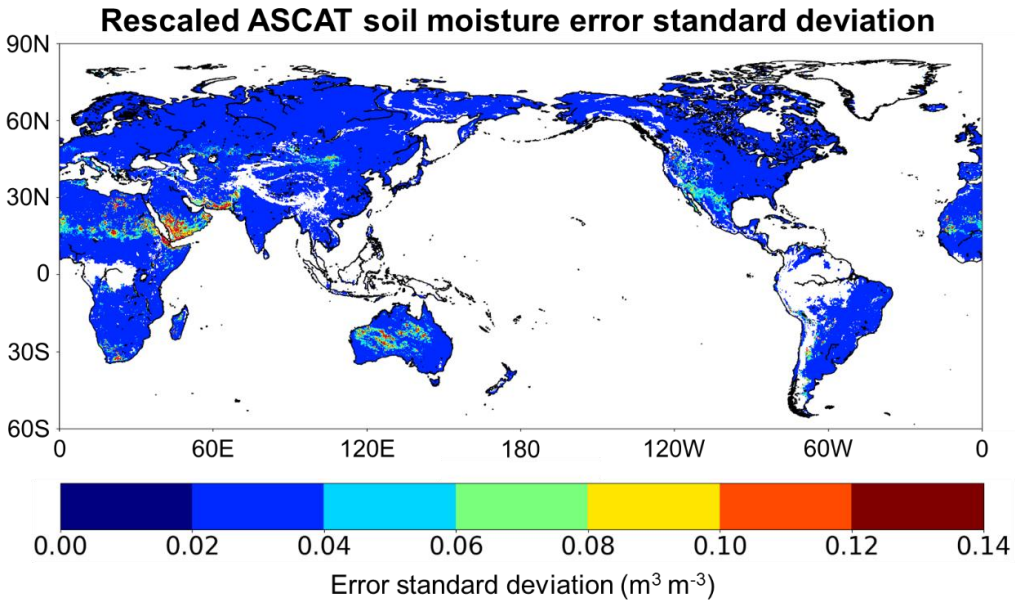

Figure 8. ASCAT soil moisture error standard deviations used for ASCAT soil moisture data assimilation (DA) in this study. The spatially distributed ASCAT soil moisture errors (m^3 m^{-3}) are derived by rescaling the constant 10% soil wetness index using the ratio of the standard deviations of the Noah land surface model (LSM) and ASCAT soil moisture time series.

The use of pre-generated spatial or spatiotemporal observation error estimates (e.g., Kim et al., 2025) can potentially maximize the benefits of each soil moisture product in multi-sensor soil moisture DA systems. One critical issue, however, is that bias correction of soil moisture observations, an essential procedure in soil moisture DA, may substantially alter their error characteristics, especially when rescaling-based methods like CDF matching are employed. To effectively apply spatially and temporally varying observation error estimates in multi-sensor soil moisture DA, a refined approach is needed to propagate error estimates from original soil moisture retrievals to bias-corrected soil moisture values.

9. Conclusions

This study develops and evaluates the NASA LIS-based multi-sensor soil moisture DA framework as part of the Korean Integrated Model (KIM) weather prediction system. We aim to investigate the impact of simultaneously assimilating satellite-based near-surface soil moisture retrievals from C-band active radar (ASCAT) and L-band passive radiometer (SMAP) observations on the weather prediction performance of the KIM-LIS-based land-atmosphere weakly coupled DA system. The ASCAT and SMAP soil moisture data are assimilated individually and jointly into the Noah LSM within the KIM-LIS system, and their relative and combined efficiencies in improving the global soil moisture analysis and atmospheric analysis/forecast skills are evaluated. Soil moisture DA is conducted using the 1-dimensional EnKF while atmospheric DA is implemented using the hybrid 4DEnVar method with 4DIAU. The experiments are performed in the global domain based on 6-hour cycling runs, which include analysis and forecast, followed by 5-day predictions at 00 UTC and 12 UTC cycles.

TCA-based evaluations indicate that assimilating either ASCAT or SMAP soil moisture data results in an overall positive effect on the global soil moisture analysis skill of the Noah LSM (i.e., 4.0% and 10.5% improvements, respectively, in the global mean performance). Both single-sensor soil moisture DA cases (i.e., SG_AT and SG_SP) enhance the soil moisture performance across land cover types, with the greatest performance gains observed in croplands. It should be noted that although this study employs the TCA method as an alternative global-scale soil moisture evaluation approach, it has limitations, particularly in constructing TCA triplets for the multi-sensor soil moisture DA experiment without violating

1005 underlying assumptions. Therefore, we applied TCA only to the single-sensor DA
1006 experiments, and the overall benefit of assimilating both sensors simultaneously can only be
1007 inferred from the single-sensor results and the atmospheric evaluation. Future studies should
1008 address this limitation to enable a more complete and robust assessment of the impact of
1009 multi-sensor soil moisture DA by implementing instrumental variable (IV)-based methods for
1010 estimating cross-correlated soil moisture errors, which require only two independent soil
1011 moisture datasets (Dong et al., 2020).

1012 Domain-averaged vertical profile RMSD metrics of the resulting atmospheric variables
1013 show that better specific humidity and air temperature analyses in the lower atmosphere are
1014 achieved with SMAP DA and ASCAT DA, respectively. Compared to the single-sensor soil
1015 moisture DA experiments, assimilating the ASCAT and SMAP soil moisture retrievals
1016 together (MT_ATSP) yields balanced skill enhancements, improving both specific humidity
1017 and air temperature analyses. Evaluations indicate that soil moisture DA within the KIM-LIS
1018 coupled system is particularly effective for the 2-m air temperature analysis and forecast,
1019 especially in the multi-sensor soil moisture DA experiment. The synergistic benefits of
1020 simultaneously assimilating both soil moisture products are regionally dependent, yielding
1021 the greatest advantage when both soil moisture products have a positive impact.

1022 In offline land DA systems, soil moisture DA typically reduces the uncertainty in
1023 modeled surface soil moisture arising mainly from errors in precipitation forcing data. Our
1024 experiments demonstrate that, in a land-atmosphere coupled system, precipitation forecast
1025 skill can also be gained from soil moisture DA through land-atmosphere interaction processes,
1026 particularly when multiple soil moisture products from diverse sources are utilized together.

Specifically, MT_ATSP improves the prediction of precipitation events, as evaluated using the ETS metric, across the range of precipitation intensity thresholds.

This study suggests that simultaneously assimilating the ASCAT and SMAP soil moisture products within the KIM-LIS coupled system can leverage their complementary advantages, as demonstrated for the estimates of specific humidity, air temperature, and precipitation. The findings obtained in this study are promising for three main reasons. First, clear synergistic local skill improvements from multi-sensor DA are evident, particularly in regions and periods where both single-sensor experiments show positive impacts. Second, the magnitude of atmospheric forecast skill improvements from both single- and multi-sensor soil moisture DA, relative to CTL, is comparable to improvements reported in previous studies (e.g., Draper and Reichle, 2019; Lin and Pu, 2019; Muñoz-Sabater et al., 2019; Reichle et al., 2023), with multi-sensor DA yielding slightly better (though not statistically significant) performance. Achieving consistent improvements across the globe remains challenging due to factors discussed in Section 8, which can cause local skill degradations in atmospheric estimates. Finally, as emphasized above, simultaneous assimilation of ASCAT and SMAP produces a more balanced improvement across atmospheric variables than single-sensor DA. These results highlight the value of assimilating soil moisture observations from multiple sensors, even if trade-offs remain for certain variables in regions or periods where single-sensor impacts conflict.

To conclude, a key aspect of this study is the joint assimilation of individual radar- and radiometer-based soil moisture products. Compared to assimilating pre-blended soil moisture data, this approach is advantageous because (1) it accounts for the relative uncertainties of

both sensors, which vary across space and time; (2) it provides a flexible framework for incorporating various combinations of soil moisture data sources within DA systems; and (3) it is more suitable for near-real time operational forecast systems, the focus of this study, since soil moisture data blending processes may increase latency and thereby reduce data availability for operational use. However, it is acknowledged that overall domain-averaged improvements in atmospheric estimates through multi-sensor soil moisture DA, relative to single-sensor DA, are still marginal and statistically insignificant. The following issues remain to be addressed in future studies to enhance future performance. First, the impact of subsurface scattering on the quality of the ASCAT soil moisture product under dry soil conditions needs to be considered in quality control procedures. Second, an alternative soil moisture bias correction method, especially for ASCAT data, should be explored. Lastly, more realistic spatially or spatiotemporally distributed estimates of soil moisture observation errors are required to maximize the benefits of multi-sensor soil moisture DA. In addition, as discussed in several previous studies, addressing biases in the soil moisture-latent heat flux coupling in LSMs (Crow et al., 2023; Kwon et al., 2024; Lei et al. 2018), accounting for the background error covariance between atmospheric and land variables during DA (Kwon et al., 2024), and assimilating screen-level observations (de Rosnay et al., 2013; Lin and Pu, 2020) can improve the positive impacts of soil moisture DA on atmospheric forecast in coupled systems.

Appendix A: Abbreviations

AMSR2	Advanced Microwave Scanning Radiometer 2
AMSU-A	Advanced Microwave Sounding Unit-A
AMVs	Atmospheric Motion Vectors
ASCAT	Advanced SCATterometer
ATMS	Advanced Technology Microwave Sounder
CDF	Cumulative distribution function
CDR	Climate Data Record
CPC	Climate Prediction Center
CrIS	Cross-track Infrared Sounder
CTL	Control case serving as a baseline experiment
DA	Data assimilation
DCA	Dual Channel Algorithm
EASE	Equal Area Scalable Earth
ECMWF	European Centre for Medium-Range Weather Forecasts
EnKF	Ensemble Kalman filter
ERA5	Fifth generation of the ECMWF atmospheric reanalysis
ESA CCI	European Space Agency Climate Change Initiative
ESME	Estimated Soil Moisture Error
ETS	Equitable threat score
EUMETSAT	European Organisation for the Exploitation of Meteorological Satellites
FAO	Food and Agriculture Organization
FB	Frequency bias
fMSE	Fractional mean-square error
GLDAS	Global Land Data Assimilation System
GPS-RO	Global Positioning System Radio Occultation
Hybrid 4DEnVar	Hybrid four-dimensional ensemble variational
IASI	Infrared Atmosphere Sounding Interferometer
IFS	Integrated Forecasting System
IGBP	International Geosphere-Biosphere Programme
KIAPS	Korea Institute of Atmospheric Prediction Systems
KIM	Korean Integrated Model
KPOP	KIM Package of Observation Processing
KVAR	KIM VARiational data assimilation
LETKF	Local ensemble transform Kalman filter
LIS	Land Information System
LPRM	Land Parameter Retrieval Model
LSM	Land surface model
LST	Local solar time
L2	Level 2

MetOp	Meteorological Operational
MHS	Microwave Humidity Sounder
MODIS	Moderate resolution imaging spectroradiometer
MT_ATSP	Multi-sensor soil moisture data assimilation experiment
NASA	National Aeronautics and Space Administration
NCEP	National Centers for Environmental Prediction
NOAA	National Oceanic and Atmospheric Administration
NSIDC	National Snow and Ice Data Center
NWP	Numerical weather prediction
RFI	Radio Frequency Interference
RMSD	Root mean square difference
SG_AT	Single-sensor data assimilation experiment using the ASCAT soil moisture data
SG_SP	Single-sensor data assimilation experiment using the SMAP soil moisture data
SMAP	Soil Moisture Active Passive
SMOS	Soil Moisture and Ocean Salinity
SMOS-IC	SMOS-INRA-CESBIO
SRTM	Shuttle Radar Topography Mission
STATSGO	State Soil Geographic
TCA	Triple collocation analysis
TU Wien	Vienna University of Technology
UTC	Coordinated Universal Time
VV	Vertical transmit vertical receive
WMO	World Meteorological Organization
4DIAU	Four-dimensional incremental analysis update

Code and data availability

The NASA Land Information System (LIS) framework is publicly available at https://github.com/NASA-LIS/LISF. Satellite-based soil moisture data assimilated in this study, i.e., Soil Moisture Active Passive (SMAP) and Advanced SCATterometer (ASCAT), can be obtained from https://n5eil01u.ecs.nsidc.org/SMAP/SPL2SMP.009/ and https://eoportal.eumetsat.int, respectively. Other global soil moisture products, used as TCA triplet components to evaluate soil moisture estimates, can be downloaded from https://www.earthdata.nasa.gov/sensors/amsr2 for the Advanced Microwave Scanning

Radiometer 2 (AMSR2) and https://ib.remote-sensing.inrae.fr/index.php/smos-ic-v2-product-documentation for the Soil Moisture and Ocean Salinity (SMOS) mission. Integrated Forecasting System (IFS) analysis data can be obtained from the European Centre for Medium-Range Weather Forecasts (ECMWF) in accordance with their data policy. The National Oceanic and Atmospheric Administration (NOAA) Climate Prediction Center (CPC) gauge-based global daily precipitation data can be downloaded from https://psl.noaa.gov/data/gridded/data.cpc.globalprecip.html. The Korean Integrated Model (KIM) software is not yet publicly available and cannot be distributed due to the Korean government's security policy. All experimental data generated in this work will be available from the authors upon request.

Author contribution

YK: conceptualization, methodology, investigation, formal analysis, writing (original draft), writing (review and editing). SJ: data curation, methodology, writing (review and editing). HK: data curation, methodology, validation, writing (review and editing). KHS: validation, writing (review and editing). IHK: supervision, methodology, writing (review and editing). EK: validation, writing (review and editing). SC: validation, writing (review and editing)

Competing interests

The contact author has declared that none of the authors has any competing interests.

Acknowledgments

This work was supported by the Korea Meteorological Administration R&D project "Development of a Next-Generation Data Assimilation System by the Korea Institute of Atmospheric Prediction Systems (KIAPS)" (KMA2020-02211). We sincerely thank the scientists of the NASA LIS team for their considerable efforts in developing the LIS framework and making it publicly available. We would also like to express our gratitude to the research teams of ECMWF, ASCAT, SMAP, AMSR2, SMOS, and NOAA CPC for sharing the data used in this study.

References

Al-Yaari, A., Wigneron, J.-P., Dorigo, W., Colliander, A., Pellarin, T., Hahn, S., Mialon, A., Richaume, P., Fernandez-Moran, R., Fan, L., Kerr, Y.H., De Lannoy, G., 2019. Assessment and inter-comparison of recently developed/reprocessed microwave satellite soil moisture products using ISMN ground-based measurements. Remote Sens. Environ. 224, 289–303. https://doi.org/10.1016/j.rse.2019.02.008.

Assouline, S., 2013. Infiltration into soils: conceptual approaches and solutions. Water Resour. Res. 49, 1755–1772. http://dx.doi.org/10.1002/wrcr.20155.

Azimi, S., Dariane, A.B., Modanesi, S., Bauer-Marschallinger, B., Bindlish, R., Wagner, W., Massari, C., 2020. Assimilation of Sentinel 1 and SMAP – based satellite soil moisture retrievals into SWAT hydrological model: the impact of satellite revisit time and product spatial resolution on flood simulations in small basins. J. Hydrol. 581, 124367. https://doi.org/10.1016/j.jhydrol.2019.124367.

Bartalis, Z., Wagner, W., Naeimi, V., Hasenauer, S., Scipal, K., Bonekamp, H., Figa, J., Anderson, C., 2007. Initial soil moisture retrievals from the METOP-A Advanced Scatterometer (ASCAT). Geophys. Res. Lett. 34, L20401. https://doi.org/10.1029/2007GL031088.

Baugh, C., de Rosnay, P., Lawrence, H., Jurlina, T., Drusch, M., Zsoter, E., Prudhomme, C., 2020. The impact of SMOS soil moisture data assimilation within the operational Global Flood Awareness System (GloFAS). Remote Sens. 12, 1490. https://doi.org/10.3390/rs12091490.

Beljaars, A.C.M., Viterbo, P., Miller, M.J., Betts, A. K., 1996. The anomalous rainfall over the United States during July1993: Sensitivity to land surface parameterization and soil moisture anomalies. Mon. Weather Rev. 124, 362–383. https://doi.org/10.1175/1520-0493(1996)124<0362:TAROTU>2.0.CO;2.

Ben Bouallègue, Z., Clare, M.C.A., Magnusson, L., Gascón, E., Maier-Gerber, M., Janoušek, M., Rodwell, M., Pinault, F., Dramsch, J.S., Lang, S.T.K., Raoult, B., Rabier, F., Chevallier, M., Sandu, I., Dueben, P., Chantry, M., Pappenberger, F., 2024. A first statistical assessment of machine learning-based weather forecasts in an operational-like context. B. Am. Meteorol. Soc. 105, E864–E883. https://doi.org/10.1175/BAMS-D-23-0162.1.

Bhuiyan, H., McNairn, H., Powers, J., Friesen, M., Pacheco, A., Jackson, T. J., Cosh, M. H., Colliander, A., Berg, A., Rowlandson, T., Bullock, P., Magagi, R., 2018. Assessing SMAP soil moisture scaling and retrieval in the carman (Canada) study site. Vadose Zone J. 17, 180132. https://doi.org/10.2136/vzj2018.07.0132.

Blyverket, J., Hamer, P.D., Bertino, L., Albergel, C., Fairbairn, D., Lahoz, W.A., 2019. An evaluation of the EnKF vs. EnOI and the assimilation of SMAP, SMOS and ESA CCI soil moisture data over the contiguous US. Remote Sens. 11, 478. https://doi.org/10.3390/rs11050478.

Bolten, J.D., Crow, W.T., Zhan, X., Jackson, T.J., Reynolds, C.A., 2010. Evaluating the utility of remotely sensed soil moisture retrievals for operational agricultural drought monitoring, IEEE J. Sel. Top. Appl. Earth Obs. Remote Sens. 3, 57–66. https://doi.org/10.1109/JSTARS.2009.2037163.

Bosilovich, M.G., Sun, W.-Y., 1999 Numerical simulation of the 1993 Midwestern flood: Land–atmosphere interactions. J. Climate 12, 1490–1505. https://doi.org/10.1175/1520-0442(1999)012<1490:NSOTMF>2.0.CO;2.

Brocca, L., Melone, F., Moramarco, T., Wagner, W., Naeimi, V., Bartalis, Z., Hasenauer, S., 2010. Improving runoff prediction through the assimilation of the ASCAT soil moisture product. Hydrol. Earth Syst. Sci. 14, 1881–1893. http://dx.doi.org/10.5194/hess-14-1881-2010.

Catalano, F., Alessandri, A., De Felice, M., Zhu, Z., Myneni, R.B., 2016. Observationally based analysis of land–atmosphere coupling. Earth Syst. Dynam. 7, 251–266. https://doi.org/10.5194/esd-7-251-2016.

Chan, S., Dunbar, R.S., 2021. Soil Moisture Active Passive (SMAP) mission: Level 2 passive soil moisture product specification document. JPL D-72547, NASA Jet Propulsion Laboratory, California, United States. https://nsidc.org/sites/default/files/d7254720smap20l2_sm_p20psd20_version2080_final.pdf.

Chan, S.K., Bindlish, R., O'Neill, P., Jackson, T., Njoku, E., Dunbar, S., Chaubell, J., Piepmeier, J., Yueh, S., Entekhabi, D., Colliander, A., Chen, F., Cosh, M.H., Caldwell, T., Walker, J., Berg, A., McNairn, H., Thibeault, M., Martínez-Fernández, J., Uldall, F., Seyfried, M., Bosch, D., Starks, P., Holifield Collins, C., Prueger, J., van der Velde, R., Asanuma, J., Palecki, M., Small, E.E., Zreda, M., Calvet, J., Crow, W.T., Kerr, Y., 2018. Development and assessment of the SMAP enhanced passive soil moisture product. Remote Sens. Environ. 204, 931–941. https://doi.org/10.1016/j.rse.2017.08.025.

Chaubell, M.J., Yueh, S.H., Dunbar, R.S., Colliander, A., Chen, F., Chan, S.K., Entekhabi, D., Bindlish, R., O'Neill, P.E., Asanuma, J., Berg, A.A., Bosch, D.D., Caldwell, T., Cosh,

M.H., Collins, C.H., Martínez-Fernández, J., Seyfried, M., Starks, P.J., Su, Z., Thibeault, M., Walker, J., 2020. Improved SMAP dual-channel algorithm for the retrieval of soil moisture. IEEE Trans. Geosci. Remote Sens. 58, 3894–3905. https://doi.org/10.1109/tgrs.2019.2959239.

Chen, M., Shi, W., Xie, P., Silva, V.B.S., Kousky, V.E., Higgins, R.W., Janowiak, J.E., 2008. Assessing objective techniques for gauge-based analyses of global daily precipitation. J. Geophys. Res. 113, D04110. https://doi.org/10.1029/2007JD009132.

Cho, E., Kwon, Y., Kumar, S.V., Vuyovich, C.M., 2023. Assimilation of airborne gamma observations provides utility for snow estimation in forested environments. Hydrol. Earth Syst. Sci. 27, 4039–4056. https://doi.org/10.5194/hess-27-4039-2023.

Colliander, A., Jackson, T.J., Bindlish, R., Chan, S., Das, N., Kim, S. B. et al., 2017. Validation of SMAP surface soil moisture products with core validation sites. Remote Sens. Environ. 191, 215–231. https://doi.org/10.1016/j.rse.2017.01.021.

Cook, B.I., Bonan, G.B., Levis, S., 2006. Soil moisture feedbacks to precipitation in southern Africa. J. Climate 19, 4198–4206. https://doi.org/10.1175/JCLI3856.1.

Crow, W.T., Van den Berg, M.J., 2010. An improved approach for estimating observation and model error parameters in soil moisture data assimilation. Water Resour. Res. 46, W12519. https://doi.org/10.1029/2010WR009402.

Crow, W.T., Kim, H., Kumar, S., 2023. Systematic modelling errors undermine the application of land data assimilation systems for hydrological and weather forecasting. J. Hydrometeor. 25, 3–26. https://doi.org/10.1175/JHM-D-23-0069.1.

Dare, R.A., Ebert, E.E., 2017. Latitudinal variations in the accuracy of model-generated forecasts of precipitation over Australia and south-east Asia. J. South. Hemisph. Earth Syst. Sci. 67, 46–63. https://doi.org/10.1071/ES17005.

Das, N.N., Entekhabi, D., Dunbar, R.S., Chaubell, M.J., Colliander, A., Yueh, S., Jagdhuber, T., Chen, F., Crow, W., O'Neill, P.E., Walker, J.P., Berg, A., Bosch, D.D., Caldwell, T., Cosh, M.H., Collins, C.H., Lopez-Baeza, E., Thibeault, M., 2019. The SMAP and Copernicus Sentinel-1A/B microwave active passive high resolution surface soil moisture product. Remote Sens. Environ. 233, 111380. https://doi.org/10.1016/j.rse.2019.111380.

Dee, D.P., Da Silva, A.M., 1998. Data assimilation in the presence of forecast bias. Quart. J. Roy. Meteor. Soc. 124, 269–295. https://doi.org/10.1002/qj.49712454512.

de Rosnay, P., Drusch, M., Vasiljevic, D., Balsamo, G., Albergel, C., Isaksen, L., 2013. A simplified extended Kalman filter for the global operational soil moisture analysis at ECMWF. Q. J. Roy. Meteor. Soc. 139, 1199–1213. https://doi.org/10.1002/qj.2023.

de Rosnay, P., Browne, P., de Boisséson, E., Fairbairn, D., Hirahara, Y. et al., 2022. Coupled data assimilation at ECMWF: current status, challenges and future developments. Q. J. Roy. Meteor. Soc. 148, 2672–2702. https://doi.org/10.1002/qj.4330.

Dirmeyer, P., Halder, S., 2016. Sensitivity of numerical weather forecasts to initial soil moisture variations in CFSv2. Wea. Forecasting 31, 1973–1983. https://doi.org/10.1175/WAF-D-16-0049.1.

Dobson, M.C., Ulaby, F.T., 1986. Active microwave soil moisture research. IEEE Trans. Geosci. Remote Sens. GE-24, 23–36. https://doi.org/10.1109/TGRS.1986.289585.

Dong, J., Wei, L., Chen, X., Duan, Z., Lu, Y., 2020. An instrument variable based algorithm for estimating cross-correlated hydrological remote sensing errors. J. Hydrol. 581, 124413. https://doi.org/10.1016/j.jhydrol.2019.124413.

Dorigo, W.A., Scipal, K., Parinussa, R.M., Liu, Y.Y., Wagner, W., De Jeu, R.A.M., Naeimi, V., 2010. Error characterisation of global active and passive microwave soil moisture datasets. Hydrol. Earth Syst. Sci. 14, 2605–2616. https://doi.org/10.5194/hess-14-2605-2010.

Dorigo, W., Wagner, W., Albergel, C., Albrecht, F., Balsamo, G., Brocca, L., Chung, D., Ertl, M., Forkel, M., Gruber, A., Haas, E., Hamer, P.D., Hirschi, M., Ikonen, J., de Jeu, R., Kidd, R., Lahoz, W., Liu, Y.Y., Miralles, D., Mistelbauer, T., Nicolai-Shaw, N., Parinussa, R., Pratola, C., Reimer, C., van der Schalie, R., Seneviratne, S.I., Smolander, T., Lecomte, P., 2017. ESA CCI soil moisture for improved Earth system understanding: state-of-the art and future directions. Remote Sens. Environ. 203, 185–215. https://doi.org/10.1016/j.rse.2017.07.001.

Draper, C.S., Mahfouf, J.-F., Walker, J.P., 2011. Root-zone soil moisture from the assimilation of screen-level variables and remotely sensed soil moisture. J. Geophys. Res. 116, D02127. https://doi.org/10.1029/2010JD013829.

Draper, C.S., Reichle, R.H., De Lannoy, G.J.M., Liu, Q., 2012. Assimilation of passive and active microwave soil moisture retrievals. Geophys. Res. Lett. 39, L04401. https://doi.org/10.1029/2011GL050655.

Draper, C., Reichle, R., de Jeu, R., Naeimi, V., Parinussa, R., Wagner, W., 2013. Estimating root mean square errors in remotely sensed soil moisture over continental scale domains. Remote Sens. Environ. 137, 288–298. https://doi.org/10.1016/j.rse.2013.06.013.

Draper, C., Reichle, R.H., 2019. Assimilation of satellite soil moisture for improved atmospheric reanalyses. Mon. Weather Rev. 147, 2163–2188. https://doi.org/10.1175/MWR-D-18-0393.1.

Drusch, M., Viterbo, P., 2007. Assimilation of screen-level variables in ECMWF's Integrated Forecast System: A study on the impact on the forecast quality and analyzed soil moisture. Mon. Weather Rev. 135, 300–314. https://doi.org/10.1175/MWR3309.1.

ECMWF, 2017. IFS Documentation CY43R3 - Part II: Data assimilation. European Centre for Medium-Range Weather Forecasts, Reading, UK, 103 pp. https://doi.org/10.21957/v61kmv92i.

Ek, M.B., Mitchell, K.E., Lin, Y., Rogers, E., Grunmann, P., Koren, V., Gayno, G., Tarpley, J.D., 2003. Implementation of Noah land surface model advances in the National Centers for Environmental Prediction operational mesoscale Eta model. J. Geophys. Res. 108, 8851. https://doi.org/10.1029/2002JD003296.

Entekhabi, D., Njoku, E.G., O'Neill, P.E., Kellogg, K.H., Crow, W.T., Edelstein, W.N., 2010. The soil moisture active passive (SMAP) mission. Proc. IEEE 98, 704–716. https://doi.org/10.1109/JPROC.2010.2043918.

Evensen, G., 1994. Sequential data assimilation with a nonlinear quasi-geostrophic model using Monte Carlo methods to forecast error statistics. J. Geophys. Res. 99, 10143–10162. https://doi.org/10.1029/94JC00572.

Fairbairn, D., de Rosnay, P., Weston, P., 2024. Evaluation of an adaptive soil moisture bias correction approach in the ECMWF land data assimilation system. Remote Sens. 16, 493. https://doi.org/10.3390/rs16030493.

Farr, T.G., Rosen, P.A., Caro, E., Crippen, R., Duren, R., Hensley, S., Kobrick, M., Paller, M., Rodriguez, E., Roth, L., Seal, D., Shaffer, S., Shimada, J., Umland, J., Werner, M., Oskin, M., Burbank, D., Alsdorf, D., 2007. The shuttle radar topography mission. Rev. Geophys. 45, RG2004. https://doi.org/10.1029/2005RG000183.

Federico, S., Torcasio, R.C., Popova, J., Sokol, Z., Pop, L., Lagasio, M., Lynn, B.H., Puca, S., Dietrich, S., 2024. Improving the lightning forecast with the WRF model and lightning data assimilation: Results of a two-seasons numerical experiment over Italy. Atmos. Res. 304, 107382. https://doi.org/10.1016/j.atmosres.2024.107382.

Ferguson, C.R., Agrawal, S., Beauharnois, M.C., Xia, G., Burrows, D.A., Bosart, L.F., 2020. Assimilation of satellite-derived soil moisture for improved forecasts of the great plains low-level jet. Mon. Weather Rev. 148, 4607–4627. https://doi.org/10.1175/MWR-D-20-0185.1.

Findell, K.L., Eltahir, E.A.B., 2003. Atmospheric controls on soil moisture–boundary layer interactions. Part I: Framework development. J. Hydrometeor. 4, 552–569. https://doi.org/10.1175/1525-7541(2003)004<0552:ACOSML>2.0.CO;2.

Friedl, M.A., McIver, D.K., Hodges, J.C.F., Zhang, X.Y., Muchoney, D., Strahler, A.H., Woodcock, C.E., Gopal, S., Schneider, A., Cooper, A., Baccini, A., Gao, F., Schaaf, C., 2002. Global land cover mapping from MODIS: algorithms and early results. Remote Sens. Environ. 83, 287–302. https://doi.org/10.1016/S0034-4257(02)00078-0.

Fuentes, I., Padarian, J., Vervoort, R.W., 2022. Towards near real-time national-scale soil water content monitoring using data fusion as a downscaling alternative. J. Hydrol. 609, 127705. https://doi.org/10.1016/j.jhydrol.2022.127705.

Gaspari, G., Cohn, S.E., 1999. Construction of correlation functions in two and three dimensions. Q. J. Roy. Meteor. Soc. 125, 723–757. https://doi.org/10.1002/qj.49712555417.

Gavahi, K., Abbaszadeh, P., Moradkhani, H., 2022. How does precipitation data influence the land surface data assimilation for drought monitoring? Sci. Total Environ. 831, 154916. https://doi.org/10.1016/j.scitotenv.2022.154916.

Gentine, P., Polcher, J., Entekhabi, D., 2011. Harmonic propagation of variability in surface energy balance within a coupled soil–vegetation–atmosphere system. Water Resour. Res. 47, W05525. http://dx.doi.org/10.1029/2010WR009268.

Gruber, A., Su, C.-H., Zwieback, S., Crow, W., Dorigo, W., Wagner, W., 2016. Recent advances in (soil moisture) triple collocation analysis. Int. J. Appl. Earth Obs. 45, 200–211. https://doi.org/10.1016/j.jag.2015.09.002.

Hersbach, H., Bell, B., Berrisford, P., Hirahara, S., Horányi, A., Muñoz-Sabater, J., Nicolas, J., Peubey, C., Radu, R., Schepers, D., et al., 2020. The ERA5 global reanalysis, Q. J. Roy. Meteorol. Soc. 146, 1999–2049. https://doi.org/10.1002/qj.3803.

Hohenegger, C., Brockhaus, P., Bretherton, C.S., Schär, C., 2009. The soil moisture–precipitation feedback in simulations with explicit and parameterized convection. J. Climate 22, 5003–5020. https://doi.org/10.1175/2009JCLI2604.1.

Hong, S.-Y., Kwon, Y.C., Kim, T.-H., Kim, J.-E.E., Choi, S.-J., Kwon, I.-H., Kim, J., Lee, E.-H., Park, R.-S., and Kim, D.-I., 2018. The Korean Integrated Model (KIM) system for global weather forecasting. Asia-Pac. J. Atmos. Sci. 54, 267–292. https://doi.org/10.1007/s13143-018-0028-9.

Huang, S., Zhang, X., Wang, C., Chen, N., 2023. Two-step fusion method for generating 1 km seamless multi-layer soil moisture with high accuracy in the Qinghai-Tibet plateau. ISPRS J. Photogramm. 197, 346–363. https://doi.org/10.1016/j. isprsjprs.2023.02.009.

Huang, S., Zhang, X., Chen, N., Ma, H., Fu, P., Dong, J., Gu, X., Nam, W.-H., Xu, L., Rab, G., Niyogi, D., 2022. A novel fusion method for generating surface soil moisture data with high accuracy, high spatial resolution, and high spatiotemporal continuity. Water Resour. Res. 58, e2021WR030827. https://doi.org/10.1029/2021WR030827.

Jalilvand, E., Tajrishy, M., Hashemi, S.A.G.Z., Brocca, L., 2019. Quantification of irrigation water using remote sensing of soil moisture in a semi-arid region. Remote Sens. Environ. 231, 111226. https://doi.org/10.1016/j.rse.2019.111226.

Jiang, M., Qiu, T., Wang, T., Zeng, C., Zhang, B., Shen, H., 2025. Seamless global daily soil moisture mapping using deep learning based spatiotemporal fusion. Int. J. Appl. Earth Obs. 139, 104517. https://doi.org/10.1016/j.jag.2025.104517.

Jun, S., Park, J.-H., Choi, H.-J., Lee, Y.-H., Lim, Y.-J., Boo, K.-O., Kang, H.-S., 2021. Impact of soil moisture data assimilation on analysis and medium-range forecasts in an operational global data assimilation and prediction system. Atmosphere 12, 1089. https://doi.org/10.3390/atmos12091089.

Kang, J.-H., Chun, H.-W., Lee, S., Ha, J.-H., Song, H.-J., Kwon, I.-H., Han, H.-J., Jeong, H., Kwon, H.-N., Kim, T.-H., 2019. Development of an observation processing package for data assimilation in KIAPS. Asia-Pac. J. Atmos. Sci. 54, 303–318. https://doi.org/10.1007/s13143-018-0030-2.

Keppenne, C.L., 2000. Data assimilation into a primitive-equation model with a parallel ensemble Kalman filter. Mon. Weather Rev. 128, 1971–1981. https://doi.org/10.1175/1520-0493(2000)128<1971:DAIAPE>2.0.CO;2.

Kerr, Y.H., Waldteufel, P., Richaume, P., Wigneron, J.P., Ferrazzoli, P., Mahmoodi, A., Al Bitar, A., Cabot, F., Gruhier, C., Juglea, S.E., Leroux, D., Mialon, A., Delwart, S., 2012. The SMOS soil moisture retrieval algorithm. IEEE Trans. Geosci. Remote Sens. 50, 1384–1403. https://doi.org/10.1109/TGRS.2012.2184548.

Khaki, M., Awange, J., 2019. The application of multi-mission satellite data assimilation for studying water storage changes over South America. Sci. Total Environ. 647, 1557–1572. https://doi.org/10.1016/j.scitotenv.2018.08.079.

Khaki, M., Hendricks Franssen, H.-J., Han, S.C., 2020. Multi-mission satellite remote sensing data for improving land hydrological models via data assimilation. Sci. Rep. 10, 18791. https://doi.org/10.1038/s41598-020-75710-5.

Khaki, M., Hoteit, I., Kuhn, M., Forootan, E., Awange, J., 2019. Assessing data assimilation frameworks for using multi-mission satellite products in a hydrological context. Sci. Total Environ. 647, 1031–1043. https://doi.org/10.1016/j.scitotenv.2018.08.032.

Kim, H., Parinussa, R., Konings, A.G., Wagner, W., Cosh, M.H., Lakshmi, V., Zohaib, M., Choi, M., 2018. Global-scale assessment and combination of SMAP with ASCAT

(active) and AMSR2 (passive) soil moisture products. Remote Sens. Environ. 204, 260–275. https://doi.org/10.1016/j.rse.2017.10.026.
Kim, H., Wigneron, J.-P., Kumar, S., Dong, J., Wagner, W., Cosh, M.H., Bosch, D.D., Collins, C.H., Starks, P.J., Seyfried, M., Lakshmi, V., 2020. Global scale error assessments of soil moisture estimates from microwave-based active and passive satellites and land surface models over forest and mixed irrigated/dryland agriculture regions. Remote Sens. Environ. 251, 112052. https://doi.org/10.1016/j.rse.2020.112052.
Kim, H., Lakshmi, V., Kwon, Y., Kumar, S.V., 2021a. First attempt of global-scale assimilation of subdaily scale soil moisture estimates from CYGNSS and SMAP into a land surface model. Environ. Res. Lett. 16, 074041. https://doi.org/10.1088/1748-9326/ac0ddf.
Kim, H., Lee, S., Cosh, M.H., Lakshmi, V., Kwon, Y., McCarty, G.W., 2021b. Assessment and combination of SMAP and Sentinel-1A/B-derived soil moisture estimates with land surface model outputs in the Mid-Atlantic Costal Plain, USA. IEEE Trans. Geosci. Remote Sens. 59, 991–1011. https://doi.org/10.1109/TGRS.2020.2991665.
Kim, H., Crow, W., Li, X., Wagner, W., Hahn, S., Lakshmi, V., 2023. True global error maps for SMAP, SMOS, and ASCAT soil moisture data based on machine learning and triple collocation analysis. Remote Sens. Environ. 298, 113776. https://doi.org/10.1016/j.rse.2023.113776.
Kim, S., Kim, H., Kwon, Y., Nguyen, H.H., 2025. A stand-alone framework for predicting spatiotemporal errors in satellite-based soil moisture using tree-based models and deep neural networks. Gisci. Remote Sens. (minor revision).
Kolassa, J., Reichle, R.H., Draper, C.S., 2017. Merging active and passive microwave observations in soil moisture data assimilation. Remote Sens. Environ. 191, 117–130. https://doi.org/10.1016/j.rse.2017.01.015.
Koo, M.-S., Baek, S., Seol, K.-H., Cho, K., 2017. Advances in land modeling of KIAPS based on the Noah land surface model. Asia-Pac. J. Atmos. Sci. 53, 361–373. https://doi.org/10.1007/s13143-017-0043-2.
Koster, R.D., Dirmeyer, P.A., Guo, Z., Bonan, G., Chan, E., Cox, P., Gordon, C.T., Kanae, S., Kowalczyk, E., Lawrence, D., Liu, P., Lu, C.-H., Malyshev, S., Mcavaney, B., Mitchell, K., Mocko, D., Oki, T., Oleson, K., Pitman, A., Sud, Y.C., Taylor, C.M., Verseghy, D., Vasic, R., Xue, Y., Yamada, T., 2004. Regions of strong coupling between soil moisture and precipitation. Science 305, 1138–1140. https://doi.org/10.1126/science.1100217.
Koster, R.D., Guo, Z., Yang, R., Dirmeyer, P.A., Mitchell, K., Puma, M.J., 2009. On the nature of soil moisture in land surface models. J. Clim. 22, 4322–4335. https://doi.org/10.1175/2009JCLI2832.1.
Koster, R.D., Mahanama, S.P.P., Yamada, T.J., Balsamo, G., Berg, A.A., Boisserie, M., Dirmeyer, P.A., Doblas-Reyes, F.J., Drewitt, G., Gordon, C.T., Guo, Z., Jeong, J.-H., Lawrence, D.M., Lee, W.-S., Li, Z., Luo, L., Malyshev, S., Merryfield, W.J., Seneviratne, S.I., Stanelle, T., van den Hurk, B.J.J.M., Vitart, F., Wood, E.F., 2010. Contribution of land surface initialization to subseasonal forecast skill: first results

from a multi-model experiment. Geophys. Res. Lett. 37, L02402. https://doi.org/10.1029/2009GL041677.
Kumar, S.V., Peters-Lidard, C.D., Tian, Y., Houser, P.R., Geiger, J., Olden, S., Lighty, L., Eastman, J.L., Dotu, B., Dirmeyer, P., Adams, J., Mitchell, K., Wood, E.F., Sheffield, J., 2006. Land information system: an interoperable framework for high resolution land surface modeling. Environ. Modell. Softw. 21, 1402–1415. https://doi.org/10.1016/j.envsoft.2005.07.004.
Kumar, S.V., Reichle, R.H., Peters-Lidard, C.D., Koster, R.D., Zhan, X., Crow, W.T., Eylander, J.B., Houser, P.R., 2008a. A land surface data assimilation framework using the land information system: Description and applications. Adv. Water Resour. 31, 1419–1432. https://doi.org/10.1016/j.advwatres.2008.01.013.
Kumar, S., Peters-Lidard, C., Tian, Y., Reichle, R.H., Geiger, J., Alonge, C., Eylander, J., Houser, P., 2008b. An integrated hydrologic modeling and data assimilation framework. Computer 41, 52–59. https://doi.org/10.1109/MC.2008.475.
Kumar, S.V., Reichle, R.H., Koster, R.D., Crow, W.T., Peters-Lidard, C.D., 2009. Role of subsurface physics in the assimilation of surface soil moisture observations. J. Hydrometeorol. 10, 1534–1547. https://doi.org/10.1175/2009JHM1134.1.
Kumar, S.V., Peters-Lidard, C.D., Mocko, D., Reichle, R., Liu, Y., Arsenault, K.R., Xia, Y., Ek, M., Riggs, G., Livneh, B., Cosh, M., 2014. Assimilation of remotely sensed soil moisture and snow depth retrievals for drought estimation. J. Hydrometeor. 15, 2446–2469, https://doi.org/10.1175/JHM-D-13-0132.1.
Kumar, S.V., Peters-Lidard, C.D., Santanello, J.A., Reichle, R.H., Draper, C.S., Koster, R.D., Nearing, G., Jasinski, M.F., 2015. Evaluating the utility of satellite soil moisture retrievals over irrigated areas and the ability of land data assimilation methods to correct for unmodeled processes. Hydrol. Earth Syst. Sci. 19, 4463–4478. https://doi.org/10.5194/hess-19-4463-2015.
Kumar, S.V., Dong, J., Peters-Lidard, C.D., Mocko, D., Gómez, B., 2017. Role of forcing uncertainty and background model error characterization in snow data assimilation. Hydrol. Earth Syst. Sci. 21, 2637–2647. https://doi.org/10.5194/hess-21-2637-2017.
Kumar, S.V., Dirmeyer, P.A., Peters-Lidard, C.D., Bindlish, R., Bolten, J., 2018. Information theoretic evaluation of satellite soil moisture retrievals. Remote Sens. Environ. 204, 392–400. https://doi.org/10.1016/j.rse.2017.10.016.
Kumar, S.V., Jasinski, M., Mocko, D.M., Rodell, M., Borak, J., Li, B., Beaudoing, H.K., Peters-Lidard, C.D., 2019. NCA-LDAS land analysis: Development and performance of a multisensory, multivariate land data assimilation system for the national climate assessment. J. Hydrometeorol. 20, 1571–1593. https://doi.org/10.1175/JHM-D-17-0125.1.
Kwon, I.-H., Song, H.-J., Ha, J.-H., Chun, H.-W., Kang, J.-H., Lee, S., Lim, S., Jo, Y., Han, H.-J., Jeong, H., Kwon, H.-N., Shin, S., Kim, T.-H., 2018. Development of an operational hybrid data assimilation system at KIAPS. Asia-Pac. J. Atmos. Sci. 54, 319–335. https://doi.org/10.1007/s13143-018-0029-8.
Kwon, Y., Forman, B.A., Ahmad, J.A., Kumar, S.V., Yoon, Y., 2019. Exploring the utility of machine learning-based passive microwave brightness temperature data assimilation

over terrestrial snow in High Mountain Asia. Remote Sens. 11, 2265. https://doi.org/10.3390/rs11192265.
Kwon, Y., Yoon, Y., Forman, B.A., Kumar, S.V., Wang, L., 2021. Quantifying the observational requirements of a space-borne LiDAR snow mission. J. Hydrol. 601, 126709. https://doi.org/10.1016/j.jhydrol.2021.126709.
Kwon, Y., Kumar, S.V., Navari, M., Mocko, D.M., Kemp, E.M., Wegiel, J.W., Geiger, J.V., Bindlish, R., 2022. Irrigation characterization improved by the direct use of SMAP soil moisture anomalies within a data assimilation system. Environ. Res. Lett. 17, 084006. https://doi.org/10.1088/1748-9326/ac7f49.
Kwon, Y., Jun, S., Kim, E., Seol, K.-H., Hong, S., Kwon, I.-H., Kang, J.-H., Kim, H., 2024. Improving weather forecast skill of the Korean Integrated Model by assimilating Soil Moisture Active Passive soil moisture anomalies. Q. J. Roy. Meteor. Soc. 150, 5305–5336. https://doi.org/10.1002/qj.4871.
Laiolo, P., Gabellani, S., Campo, L., Silvestro, F., Delogu, F., Rudari, R., Pulvirenti, L., Boni, G., Fascetti, F., Pierdicca, N., Crapolicchio, R., Hasenauer, S., Puca, S., 2016. Impact of different satellite soil moisture products on the predictions of a continuous distributed hydrological model. Int. J. Appl. Earth Obs. 48, 131–145. https://doi.org/10.1016/j.jag.2015.06.002.
Lamichhane, M., Mehan, S., Mankin, K.R., 2025. Surface soil moisture prediction using multimodal remote sensing data fusion and machine learning algorithms in semi-arid agricultural region. Sci. Remote Sens. 12, 100255. https://doi.org/10.1016/j.srs.2025.100255.
Lee, S., Song, H.-J., Chun, H.-W., Kwon, I.-H., Kang, J.-H., Lim, S., 2020. All-sky microwave humidity sounder assimilation in the Korean Integrated Model forecast system. Q. J. Roy. Meteor. Soc. 146, 3570-3586. https://doi.org/10.1002/qj.3862.
Lei, F., Crow, W.T., Holmes, T.R.H., Hain, C., Anderson, M.C., 2018. Global investigation of soil moisture and latent heat flux coupling strength. Water Resour. Res. 54, 8196–8215. https://doi.org/10.1029/2018WR023469.
Li, S., Zhang, L., Ma, R., Yan, M., Tian, X., 2020. Improved ET assimilation through incorporating SMAP soil moisture observations using a coupled process model: A study of U.S. arid and semiarid regions. J. Hydrol. 590, 125402. https://doi.org/10.1016/j.jhydrol.2020.125402.
Lievens, H., De Lannoy, G.J.M., Al Bitar, A., Drusch, M., Dumedah, G., Hendricks Franssen, H.-J., Kerr, Y.H., Tomer, S.K., Martens, B., Merlin, O., Pan, M., Roundy, J.K., Vereecken, H., Walker, J.P., Wood, E.F., Verhoest, N.E.C., Pauwels, V.R.N., 2016. Assimilation of SMOS soil moisture and brightness temperature products into a land surface model. Remote Sens. Environ. 180, 292–304. https://doi.org/10.1016/j.rse.2015.10.033.
Lin, X., Huang, S., Li, J., Huang, Q., Shi, H., She, D., Leng, G., Wei, X., Guo, W., Liu, Y., Luo, J., 2023. Feedback dynamics between precipitation, temperature, and soil moisture in China and their possible driving mechanisms under a changing environment. Atmos. Res. 294, 106983. https://doi.org/10.1016/j.atmosres.2023.106983.

Lin, L.-F., Pu, Z., 2019. Examining the impact of SMAP soil moisture retrievals on short-range weather prediction under weakly and strongly coupled data assimilation with WRF-Noah. Mon. Weather Rev. 147, 4345–4366. https://doi.org/10.1175/MWR-D-19-0017.1.

Lin, L.-F., Pu, Z., 2020. Improving near-surface short-range weather forecasts using strongly coupled land–atmosphere data assimilation with GSI-EnKF. Mon. Weather Rev. 148, 2863–2888. https://doi.org/10.1175/MWR-D-19-0370.1.

Liu, Q., Reichle, R.H., Bindlish, R., Cosh, M.H., Crow, W.T., de Jeu, R., De Lannoy, G.J.M., Huffman, G.J., Jackson, T.J., 2011. The contributions of precipitation and soil moisture observations to the skill of soil moisture estimates in a land data assimilation system. J. Hydrometeorol. 12, 750–765. https://doi.org/10.1175/JHM-D-10-05000.1.

Lodh, A., Routray, A., Dutta, D., George, J.P., Mitra, A.K., 2022. Improving the prediction of monsoon depressions by assimilating ASCAT soil moisture in NCUM-R modeling system. Atmos. Res. 272, 106130. https://doi.org/10.1016/j.atmosres.2022.106130.

Long, D., Bai, L., Yan, L., Zhang, C., Yang, W., Lei, H., Quan, J., Meng, X., Shi, C., 2019. Generation of spatially complete and daily continuous surface soil moisture of high spatial resolution. Remote Sens. Environ. 233, 111364. https://doi.org/10.1016/j.rse.2019.111364.

Lorenc, A.C., Bowler, N.E., Clayton, A.M., Pring, S.R., Fairbairn, D., 2015. Comparison of hybrid-4DEnVar and hybrid-4DVar data assimilation methods for global NWP. Mon. Weather Rev. 143, 212–229. https://doi.org/10.1175/MWR-D-14-00195.1.

Manco, I., De Lucia, C., Repola, F., Fedele, G., Mercogliano, P., 2023. A comparative performance study of WRF, COSMO and ICON atmospheric models for the Italian peninsula at very high resolution. Tethys 20, 1–20. https://doi.org/10.3369/tethys.2023.20.01.

Miller, D.A., White, R.A., 1998. A conterminous United States multilayer soil characteristics dataset for regional climate and hydrology modelling. Earth Interact. 2, 1–26. https://doi.org/10.1175/1087-3562(1998)002<0001:ACUSMS>2.3.CO;2.

Min, X., Shangguan, Y., Li, D., Shi, Z., 2022. Improving the fusion of global soil moisture datasets from SMAP, SMOS, ASCAT, and MERRA2 by considering the non-zero error covariance. Int. J. Appl. Earth Obs. 113, 103016. https://doi.org/10.1016/j.jag.2022.103016.

Muñoz-Sabater, J., Lawrence, H., Albergel, C., de Rosnay, P., Isaksen, L., Mecklenburg, S. et al., 2019. Assimilation of SMOS brightness temperatures in the ECMWF integrated forecasting system. Q. J. Roy. Meteor. Soc. 145, 2524–2548. https://doi.org/10.1002/QJ.3577.

Nair, A.S., Indu, J., 2018. A coupled land surface and radiative transfer models based on relief correction for a reliable land data assimilation over mountainous terrain. IEEE Geosci. Remote Sens. Lett. 15, 1657–1661. https://doi.org/10.1109/LGRS.2018.2854908.

Nair, A.S., Indu, J., 2019. Improvement of land surface model simulations over India via data assimilation of satellite-based soil moisture products. J. Hydrol. 573, 406–421. https://doi.org/10.1016/j.jhydrol.2019.03.088.

1524 Nearing, G., Yatheendradas, S., Crow, W., Zhan, X., Liu, J., Chen, F., 2018. The efficiency
1525 of data assimilation. Water Resour. Res. 54, 6374–6392.
1526 https://doi.org/10.1029/2017WR020991.
1527 Nguyen, H.H., Kim, H., Crow, W., Yueh, S., Wagner, W., Lei, F., Wigneron, J.-P.,
1528 Colliander, A., Frappart, F., 2025. From theory to hydrological practice: Leveraging
1529 CYGNSS data over seven years for advanced soil moisture monitoring. Remote Sens.
1530 Environ. 316, 114509. https://doi.org/10.1016/j.rse.2024.114509.
1531 O'Neill, P.E., Chan, S., Njoku, E.G., Jackson, T., Bindlish, R., Chaubell, J., 2021. SMAP L2
1532 radiometer half-orbit 36 km EASE-grid soil moisture, version 8 [Data Set]. Boulder,
1533 Colorado USA. NASA National Snow and Ice Data Center Distributed Active Archive
1534 Center. https://doi.org/10.5067/LPJ8F0TAK6E0. Date Accessed 06-01-2023.
1535 Orth, R., Seneviratne, S.I., 2013. Propagation of soil moisture memory to streamflow and
1536 evapotranspiration in Europe. Hydrol. Earth Syst. Sci. 17, 3895–3911.
1537 https://doi.org/10.5194/hess-17-3895-2013.
1538 Pal, J.S., Eltahir, E.A.B., 2003. A feedback mechanism between soil-moisture distribution
1539 and storm tracks. Q. J. Roy. Meteor. Soc. 129, 2279–2297.
1540 https://doi.org/10.1256/qj.01.201.
1541 Paloscia, S., Pampaloni, P., 1988. Microwave polarization index for monitoring vegetation
1542 growth. IEEE Trans. Geosci. Remote Sens. 26, 617–621.
1543 https://doi.org/10.1109/36.7687.
1544 Peters-Lidard, C.D., Houser, P.R., Tian, Y., Kumar, S.V., Geiger, J., Olden, S., Lighty, L.,
1545 Doty, B., Dirmeyer, P., Adams, J., Mitchell, K., Wood, E.F., Sheffield, J., 2007. High-
1546 performance Earth system modeling with NASA/GSFC's land information system.
1547 Innov. Syst. Softw. Eng. 3, 157–165. https://doi.org/10.1007/s11334-007-0028-x.
1548 Pipunic, R.C., Walker, J.P., Western, A.W., Trudinger, C.M., 2013. Assimilation of multiple
1549 data types for improved heat flux prediction: a one-dimensional field study. Remote
1550 Sens. Environ. 136, 315–329. http://dx.doi.org/10.1016/j.rse.2013.05.015.
1551 Polichtchouk, I., van Niekerk, A., Wedi, N., 2023. Resolved gravity waves in the
1552 extratropical stratosphere: Effect of horizontal resolution increase from O(10) to O(1)
1553 km. J. Atmos. Sci. 80, 473–486. https://doi.org/10.1175/JAS-D-22-0138.1.
1554 Reichle, R.H., McLaughlin, D.B., Entekhabi, D., 2002a. Hydrologic data assimilation with
1555 the ensemble Kalman filter. Mon. Weather Rev. 130, 103–114.
1556 https://doi.org/10.1175/1520-0493(2002)130<0103:HDAWTE>2.0.CO;2.
1557 Reichle, R.H., Walker, J.P., Koster, R.D., Houser, P.R., 2002b. Extended versus ensemble
1558 Kalman filtering for land data assimilation. J. Hydrometeorol. 3, 728–740.
1559 https://doi.org/10.1175/1525-7541(2002)003<0728:EVEKFF>2.0.CO;2.
1560 Reichle, R.H., Koster, R.D., 2004. Bias reduction in short records of satellite soil moisture.
1561 Geophys. Res. Lett. 31, L19501. https://doi.org/10.1029/2004GL020938.
1562 Reichle, R.H., Koster, R.D., Liu, P., Mahanama, S.P.P., Njoku, E.G., Owe, M., 2007.
1563 Comparison and assimilation of global soil moisture retrievals from the advanced
1564 microwave scanning radiometer for the earth observing system (AMSR-E) and the
1565 scanning multichannel microwave radiometer (SMMR). J. Geophys. Res. Atmos. 112,
1566 D09108. https://doi.org/10.1029/2006JD008033.

Reichle, R.H., Crow, W.T., Koster, R.D., Sharif, H.O., Mahanama, S.P.P., 2008. Contribution of soil moisture retrievals to land data assimilation products. Geophys. Res. Lett. 35, L01404. https://doi.org/10.1029/2007GL031986.

Reichle, R.H., Zhang, S.Q., Kolassa, J., Liu, Q., Todling, R., 2023. A weakly-coupled land surface analysis with SMAP radiance assimilation improves GEOS medium-range forecasts of near-surface air temperature and humidity. Q. J. Roy. Meteor. Soc. 149, 1867-1889. https://doi.org/10.1002/qj.4486.

Renzullo, L.J., van Dijk, A.I.J.M., Perraud, J.-M., Collins, D., Henderson, B., Jin, H., Smith, A.B., McJannet, D.L., 2014. Continental satellite soil moisture data assimilation improves root-zone moisture analysis for water resources assessment. J. Hydrol. 519, 2747–2762. https://doi.org/10.1016/j.jhydrol.2014.08.008.

Reynolds, C.A., Jackson, T.J., Rawls, W.J., 2000. Estimating soil water-holding capacities by linking the Food and Agriculture Organization Soil map of the world with global pedon databases and continuous pedotransfer functions. Water Resour. Res. 36, 3653–3662. https://doi.org/10.1029/2000WR900130.

Ricker, M., Behrens, A., Staneva, J., 2024. The operational CMEMS wind wave forecasting system of the Black Sea. J. Oper. Oceanogr. 1–22. https://doi.org/10.1080/1755876X.2024.2364974.

Rodell, M., Houser, P.R., Jambor, U., Gottschalck, J., Mitchell, K., Meng, C.-J., Arsenault, K., Cosgrove, B., Radakovich, J., Bosilovich, M., Entin, J.K., Walker, J.P., Lohmann, D., Toll, D., 2004. The Global Land Data Assimilation System. Bull. Am. Meteorol. Soc. 85, 381–394. https://doi.org/10.1175/BAMS-85-3-381.

Sacchetti, D., Cassola, F., Corazza, M., Pedemonte, L., Tizzi, M., Drofa, O., Davolio, S., 2024. The ARPAL atmospheric operational modeling chain and its applications: description and validation. Bull. Atmos. Sci. Technol. 5, 1. https://doi.org/10.1007/s42865-024-00064-z.

Santanello Jr., J.A., Kumar, S.V., Peters-Lidard, C.D., Lawston, P.M., 2016. Impact of soil moisture assimilation on land surface model spinup and coupled land–atmosphere prediction. J. Hydrometeorol. 17, 517–540. https://doi.org/10.1175/JHM-D-15-0072.1.

Schaake, J.C., Koren, V.I., Duan, Q.Y., Mitchell, K., Chen, F., 1996. A simple water balance model (SWB) for estimating runoff at different spatial and temporal scales. J. Geophys. Res. 101, 7461–7475. https://doi.org/10.1029/95JD02892.

Schmugge, T.J., O'Neill, P.E., Wang, J.R., 1986. Passive microwave soil moisture research. IEEE Trans. Geosci. Remote Sens. GE-24, 1. http://dx.doi.org/10.1109/TGRS.1986.289584.

Scipal, K., Holmes, T., De Jeu, R., Naeimi, V., Wagner, W., 2008. A possible solution for the problem of estimating the error structure of global soil moisture data sets. Geophys. Res. Lett. 35, L24403, https://doi.org/10.1029/2008GL035599.

Seo, E., Lee, M.-I., Reichle, R.H., 2021. Assimilation of SMAP and ASCAT soil moisture retrievals into the JULES land surface model using the Local Ensemble Transform Kalman Filter. Remote Sens. Environ. 253, 112222. https://doi.org/10.1016/j.rse.2020.112222.

1609 Shellito, P.J., Small, E.E., Cosh, M.H., 2016. Calibration of Noah soil hydraulic property
1610 parameters using surface soil moisture from SMOS and Basinwide in situ observations.
1611 J. Hydrometeorol. 17, 2275–2292. https://doi.org/10.1175/JHM-D-15-0153.1.
1612 Shellito, P.J., Small, E.E., Livneh, B., 2018. Controls on surface soil drying rates observed by
1613 SMAP and simulated by the Noah land surface model. Hydrol. Earth Syst. Sci. 22,
1614 1649–1663. https://doi.org/10.5194/hess-22-1649-2018.
1615 Shin, Y., Jung, Y., 2014. Development of irrigation water management model for reducing
1616 drought severity using remotely sensed soil moisture footprints J. Irrig. Drain. Eng. 140,
1617 04014021. https://doi.org/10.1061/(ASCE)IR.1943-4774.0000736.
1618 Shin, S., Kang, J.-S., Jo, Y., 2016. The local ensemble transform Kalman filter (LETKF) with
1619 a global NWP model on the cubed sphere. Pure Appl. Geophys. 173, 2555–2570,
1620 https://doi.org/10.1007/s00024-016-1269-0.
1621 Shin, S., Kang, J.-H., Chun, H.-W., Lee, S., Sung, K., Cho, K., Jo, Y., Kim, J.-E., Kwon, I.-
1622 H., Lim, S., Kang, J.-S., 2018. Real data assimilation using the Local Ensemble
1623 Transform Kalman Filter (LETKF) system for a global nonhydrostatic NWP model on
1624 the cubed-sphere. Asia-Pac. J. Atmos. Sci. 54, 351–360.
1625 https://doi.org/10.1007/s13143-018-0022-2.
1626 Singh, A., Gaurav, K., 2023. Deep learning and data fusion to estimate surface soil moisture
1627 from multi-sensor satellite images. Sci. Rep. 13, 2251. https://doi.org/10.1038/s41598-
1628 023-28939-9.
1629 Song, H.-J., Kwon, I.-H., 2015. Spectral transformation using a cubed-sphere grid for a three-
1630 dimensional variational data assimilation system. Mon. Weather Rev. 143, 2581–2599.
1631 https://doi.org/10.1175/MWR-D-14-00089.1.
1632 Song, H.-J., Shin, S., Ha, J.-H., Lim, S., 2017. The advantages of hybrid 4DEnVar in the
1633 context of the forecast sensitivity to initial conditions. J. Geophys. Res. Atmos. 122,
1634 12226–12244. https://doi.org/10.1002/2017JD027598.
1635 Stoffelen, A., 1998. Toward the true near-surface wind speed: error modeling and calibration
1636 using triple collocation. J. Geophys. Res. 103, 7755–7766.
1637 https://doi.org/10.1029/97JC03180.
1638 Tangdamrongsub, N., Han, S.-C., Yeo, I.-Y., Dong, J., Steele-Dunne, S.C., Willgoose, G.,
1639 Walker, J.P., 2020. Multivariate data assimilation of GRACE, SMOS, SMAP
1640 measurements for improved regional soil moisture and groundwater storage estimates.
1641 Adv. Water Resour. 135, 103477. https://doi.org/10.1016/j.advwatres.2019.103477.
1642 Torcasio, R.C., Mascitelli, A., Realini, E., Barindelli, S., Tagliaferro, G., Puca, S., Dietrich,
1643 S., Federico, S., 2023. The impact of global navigation satellite system (GNSS) zenith
1644 total delay data assimilation on the short-term precipitable water vapor and
1645 precipitation forecast over Italy using the Weather Research and Forecasting (WRF)
1646 model. Nat. Hazards Earth Syst. Sci. 23, 3319–3336. https://doi.org/10.5194/nhess-23-
1647 3319-2023.
1648 Tuttle, S., Salvucci, G., 2016. Empirical evidence of contrasting soil moisture–precipitation
1649 feedbacks across the United States. Science 352, 825–828.
1650 https://doi.org/10.1126/science.aaa7185.

van den Hurk, B., Doblas-Reyes, F., Balsamo, G., Koster, R.D., Seneviratne, S.I., Camargo Jr, H., 2012. Soil moisture effects on seasonal temperature and precipitation forecast scores in Europe. Climate Dyn. 38, 349–362. https://doi.org/10.1007/s00382-010-0956-2.

van der Schalie, R., de Jeu, R., Rodríguez-Fernández, N., Al-Yaari, A., Kerr, Y., Wigneron, J.-P., Parinussa, R., Drusch, M., 2018. The Effect of three different data fusion approaches on the quality of soil moisture retrievals from multiple passive microwave sensors. Remote Sens. 10, 107. https://doi.org/10.3390/rs10010107.

Wagner, W., Lemoine, G., Rott, H., 1999. A method for estimating soil moisture from ERS scatterometer and soil data. Remote Sens. Environ. 70, 191–207. https://doi.org/10.1016/S0034-4257(99)00036-X.

Wagner, W., Bartalis, Z., Naeimi, V., Park, S.-E., Figa-Saldaña, J., Bonekamp, H., 2010. Status of the MetOp ASCAT soil moisture product. IEEE Int. Geosci. Remote. Se. Proceedings. 25-30 July 2010, 276–279. https://doi.org/10.1109/IGARSS.2010.5653358.

Wagner, W., Hahn, S., Kidd, R., Melzer, T., Bartalis, Z., Hasenauer, S., Figa-Saldaña, J., De Rosnay, P., Jann, A., Schneider, S., Komma, J., Kubu, G., Brugger, K., Aubrecht, C., Züger, J., Gangkofner, U., Kienberger, S., Brocca, L., Wang, Y., Blöschl, G., Eitzinger, J., Steinnocher, K., Zeil, P., Rubel, F., 2013. The ASCAT soil moisture product: A review of its specifications, validation results, and emerging applications. Meteorologische Zeitschrift 22, 5–33. https://doi.org/10.1127/0941-2948/2013/0399.

Wagner, W., Lindorfer, R., Hahn, S., Kim, H., Vreugdenhil, M., Gruber, A., Fischer, M., Trnka, M., 2024. Global scale mapping of subsurface scattering signals impacting ASCAT soil moisture retrievals. IEEE Trans. Geosci. Remote Sens. 62, 4509520. https://doi.org/10.1109/TGRS.2024.3429550.

Wanders, N., Karssenberg, D., de Roo, A., de Jong, S.M., Bierkens, M.F.P., 2014. The suitability of remotely sensed soil moisture for improving operational flood forecasting, Hydrol. Earth Syst. Sci. 18, 2343–2357. https://doi.org/10.5194/hess-18-2343-2014.

Wang, Y., Mao, J., Jin, M., Hoffman, F.M., Shi, X., Wullschleger, S.D., Dai, Y., 2021. Development of observation-based global multilayer soil moisture products for 1970 to 2016. Earth Syst. Sci. Data 13, 4385–4405. https://doi.org/10.5194/essd-13-4385-2021.

Whitaker, J.S., Hamill, T.M., 2012. Evaluating methods to account for system errors in ensemble data assimilation. Mon. Weather Rev. 140, 3078–3089. https://doi.org/10.1175/MWR-D-11-00276.1.

WMO, 2008. Recommendations for the verification and intercomparison of QPFs and PQPFs from operational NWP models. WWRP 2009-1, World Meteorological Organization (WMO), Switzerland.

Wu, K., Ryu, D., Nie, L., Shu, H., 2021. Time-variant error characterization of SMAP and ASCAT soil moisture using Triple Collocation Analysis. Remote Sens. Environ. 256, 112324. https://doi.org/10.1016/j.rse.2021.112324.

Xie, P., Yatagai, A., Chen, M., Hayasaka, T., Fukushima, Y., Liu, C., Yang, S., 2007. A gauge-based analysis of daily precipitation over East Asia. J. Hydrometeorol. 8, 607–626. https://doi.org/10.1175/JHM583.1.

Xie, Q., Jia, L., Menenti, M., Hu, G., 2022. Global soil moisture data fusion by Triple Collocation Analysis from 2011 to 2018. Sci. Data 9, 687. https://doi.org/10.1038/s41597-022-01772-x.
Xu, T., Chen, F., He, X., Barlage, M., Zhang, Z., Liu, S., He, X., 2021. Improve the performance of the Noah-MP-Crop model by jointly assimilating soil moisture and vegetation phenology data. J. Adv. Model. Earth Sy. 13, e2020MS002394. https://doi.org/10.1029/2020MS002394.
Yang, L., Sun, G., Zhi, L., Zhao, J., 2018. Negative soil moisture-precipitation feedback in dry and wet regions. Sci. Rep. 8, 4026. https://doi.org/10.1038/s41598-018-22394-7.
Yin, J., Hain, C.R., Zhan, X., Dong, J., Ek, M., 2019. Improvements in the forecasts of near-surface variables in the Global Forecast System (GFS) via assimilating ASCAT soil moisture retrievals. J. Hydrol. 578, 124018. https://doi.org/10.1016/j.jhydrol.2019.124018.
Yuan, X., Wood, E.F., Luo, L., Pan, M., 2011. A first look at Climate Forecast System version 2 (CFSv2) for hydrological seasonal prediction. Geophys. Res. Lett. 38, L13402. https://doi.org/10.1029/2011GL047792.
Zhang, H., Wang, S., Liu, K., Li, X., Li, Z., Zhang, X., Liu, B., 2022. Downscaling of AMSR-E soil moisture over north China using random forest regression. ISPRS Int. J. Geo Inf. 11, 101. https://doi.org/10.3390/ijgi11020101.
Zheng, J., Yuan, X., Ji, P., 2024. The important role of reliable land surface model simulation in high-resolution multi-source soil moisture data fusion by machine learning. J. Hydrol. 630, 130700. https://doi.org/10.1016/j.jhydrol.2024.130700.